

Are debris disks self-stirred?

G. M. Kennedy^{*} and M. C. Wyatt

Institute of Astronomy, University of Cambridge, Madingley Road, Cambridge CB3 0HA, UK

23 February 2024

ABSTRACT

This paper aims to consider the evidence that debris disks are self-stirred by the formation of Pluto-size objects. A semi-analytical model for the dust produced during self-stirring is developed and applied to the statistics for A stars. We show that there is no significant statistical difference between fractional excesses of A-stars $\lesssim 50$ Myr old, and therefore focus on reproducing the broad trends, the “rise and fall” of the fraction of stars with excesses that the pre-stirred model of Wyatt et al. (2007b) does not predict. Using a population model, we find that the statistics and trends can be reproduced with a self-stirring model of planetesimal belts with radius distribution $N(r) \propto r^{-0.8}$ between 15–120 AU, with width $dr = r/2$. Disks must have this 15 AU minimum radius in order to show a peak in disk fraction, rather than a monotonic decline. However, the marginal significance of the peak in the observations means that models with smaller minimum radii also formally fit the data. Populations of extended disks with fixed inner and/or outer radii fail to fit the statistics, due mainly to the slow $70 \mu\text{m}$ evolution as stirring moves further out in the disk. This conclusion, that debris disks are narrow belts rather than extended disks, is independent of the significance of $24 \mu\text{m}$ trends for young A-stars. Although the rise and fall is naturally explained by self-stirring, we show that the statistics can also be reproduced with a model in which disks are stirred by secular perturbations from a nearby eccentric planet. Detailed imaging, which can reveal warps, sharp edges, and offsets in individual systems is the best way to characterise the stirring mechanism. From a more detailed look at β Pictoris Moving Group and TW Hydrae Association A-stars we find that the disk around β Pictoris is likely the result of secular stirring by the proposed planet at ~ 10 AU; the structure of the HR 4796A disk also points to sculpting by a planet. The two other stars with disks, HR 7012 and η Tel, possess transient hot dust, though the outer η Tel disk is consistent with a self-stirred origin. We suggest that planet formation provides a natural explanation for the belt-like nature of debris disks, with inner regions cleared by planets that may also stir the disk, and the outer edges set by where planetesimals can form.

Key words: circumstellar matter – stars: planetary systems: formation – stars: planetary systems: protoplanetary discs.

1 INTRODUCTION

Debris disks are the disks of dust found around nearby main sequence stars through their thermal emission (for a recent review see Wyatt 2008). The dust itself is short-lived compared to the lifetime of the star so is believed to be continually replenished through collisions between km-sized planetesimals (Wyatt & Dent 2002; Quillen et al. 2007), much in the same way that dust

in the zodiacal cloud is replenished through collisions in the asteroid belt and Kuiper belt (Dermott et al. 2001; Moro-Martín & Malhotra 2003). While there remain difficulties in growing dust from its initially sub- μm size into >km-sized planetesimals (Blum & Wurm 2008), the widely invoked coagulation and core accretion models for planet formation rely on relative velocities in the protoplanetary disk being low enough that collisions result in net accretion, rather than destruction. As it seems that the opposite is the case in debris disks, these disks must have been stirred at some point so that collisions occur at

^{*} Email: gkennedy@ast.cam.ac.uk

$\gtrsim 1\text{--}10\text{ m/s}$, which typically corresponds to eccentricities and inclinations for the disk material of $e \gtrsim 10^{-3}$ to 10^{-2} (e.g. [Kenyon & Bromley 2008](#)).

To explain debris disks it is not normally necessary to understand how (or when) they were stirred. It is sufficient to invoke a “pre-stirred” debris disk—one that was stirred when the star was born. For example, it is possible to explain the statistics of dust found around A-stars of ages $>10\text{ Myr}$ by assuming that all stars are born with a pre-stirred planetesimal belt that evolves due to steady-state collisional erosion ([Wyatt et al. 2007b](#)). The diversity seen at different ages then reflects their different initial masses and radii. A similar conclusion was reached for debris disks around sun-like stars ([Löhne et al. 2008](#)).

However, recent results on the presence of debris disks around young A-stars are challenging this view by showing that the fractional excess at $24\ \mu\text{m}$ from hot dust increases from 3 Myr (the time at which most protoplanetary disks have dissipated) to a peak at $\sim 10\text{--}30\text{ Myr}$, followed by a slow decline as expected by steady-state evolution ([Hernández et al. 2006](#); [Currie et al. 2008a,b](#)). This peak has been interpreted as evidence for self-stirring, where debris are created when the largest objects become massive enough to stir planetesimals to fragmentation velocities.¹

Self-stirring models follow the evolution of an extended planetesimal belt from the protoplanetary disk stage, allowing both the size distribution and the velocity distribution to evolve in a self-consistent manner. These models find that stirring of the planetesimal belts occurs when planets reach Pluto-size, which depends strongly on their distance from the star, as well as on the mass surface density of solid material there: $t_{\text{Pluto}} \propto P/\Sigma$, where P is the orbital period and Σ is the surface density of planetesimals (e.g. [Lissauer 1987](#)). For a typical disk model $\Sigma = \Sigma_0 r^{-1.5}$, so t_{Pluto} depends strongly on radius r :

$$t_{\text{Pluto}} \propto r^3 / \left(\Sigma_0 \sqrt{M_\star} \right). \quad (1)$$

Thus, compared to pre-stirred disks, self-stirring means that farther disk regions are stirred at later times because it takes longer for Pluto-size objects to form there. This evolution means that individual disks can show a peak in emission at $\sim 10\text{--}30\text{ Myr}$, set by the time to form Pluto-size objects at the inner disk edge ([Hernández et al. 2006](#); [Currie et al. 2008a](#); [Kenyon & Bromley 2008](#); [Wyatt 2008](#)). That is, the observed evolution occurs if debris disks tend to have $\sim 10\text{ AU}$ inner holes. The overall dust content at $<10\text{ Myr}$ is low because such times are needed for Plutos to form at the inner edge of the disk. This lack of dust implies that accretion with minimal fragmentation is ongoing in young ($<10\text{ Myr}$) debris disks and the outer regions of older debris disks.

Though the [Kenyon & Bromley \(2008\)](#) self-stirring models are qualitatively consistent with the $\sim 10\text{--}30\text{ Myr}$ peak in fractional excesses, there has been no quantitative test of whether these models can reproduce the observed A-star statistics, or how the observations constrain disk

parameters. In this paper, our aim is to address this issue using the [Wyatt et al. \(2007a\)](#) debris disk evolution model, modified to include self-stirring (as outlined in [Wyatt 2008](#)).

In particular, there are several issues to address. Because the peak in excesses occurs when Plutos form at the inner disk edge, the timing of this peak is highly dependent on the radius of the cleared region and on mass surface density (Eq. 1). Yet we know that protoplanetary disks have a range of masses and surface densities (e.g. [Natta et al. 2000](#); [Andrews & Williams 2005, 2007](#)), and it seems unlikely that the inner clearing would be at the same radius for all disks. Therefore, we wish to find whether self-stirring models can reproduce the A-star statistics, and if so, whether they put a strong constraint on disk inner radii as Equation (1) suggests.

Another issue is the extent of debris disks. [Kalas et al. \(2006\)](#) note that disks resolved in scattered light appear to be either relatively narrow belts $20\text{--}30\text{ AU}$ wide, or extended disks wider than 50 AU (however, a disk that appears extended may result from blowout of small grains created in a relatively narrow planetesimal belt). In fitting the statistics for ($\gtrsim 10\text{ Myr}$) A-stars [Wyatt et al. \(2007b\)](#) considered disks to be the former; belts centred at radial distance r with an assumed width of $dr = r/2$. However, self-stirring allows the interesting possibility that disks similar in extent to observed protoplanetary disks—from near the star to many hundreds of AU—may evolve to look like narrow belts because only regions of recent Pluto formation may be luminous enough to be detected. Therefore, we also wish to evaluate whether debris disks tend to be “narrow belts” or “extended disks” (we use these terms consistently throughout to refer to these types of disks).

A final issue is whether debris disks could be stirred by something other than the formation of Pluto-sized objects. Though self-stirring has been the only proposed mechanism, secular perturbations from planets (another subset of delayed stirring) seems to be an equally viable way to stir debris disks ([Mustill & Wyatt 2009](#)). This hypothesis is partly motivated by stars with debris disks known or predicted to harbour planets, such as Fomalhaut and $\beta\text{ Pic}$ ([Mouillet et al. 1997](#); [Quillen 2006](#); [Kalas et al. 2008](#); [Lagrange et al. 2009a](#)). The question is therefore whether we can identify the more important stirring mechanism, both at a population level and for individual objects.

The layout of this paper is as follows. In §2 we outline the [Wyatt et al. \(2007a,b\)](#) model, and the modifications made to include self-stirring. We empirically fit some model parameters to reproduce the self-stirring models of [Kenyon & Bromley \(2008\)](#) in §3. As self-stirring results in not only excess evolution, but also spatial evolution as Plutos form farther from the central star, we show how disk surface density profiles evolve and vary with model parameters. In §4 a population model is compared with the statistics for A-stars. We briefly consider a planet-stirred population model, take a more detailed look at resolved $\beta\text{ Pictoris}$ Moving Group and TW Hydrae A-stars in the context of delayed stirring, and discuss other influences on debris disk structure in §5. We summarise our main conclusions in §6.

¹ Self-stirring is also called delayed stirring in the literature, but following [Wyatt \(2008\)](#) we consider that what we are calling self-stirring is a sub-set of possible delayed-stirring models.

2 ANALYTICAL SELF-STIRRING MODEL

This section describes the analytical model. It is an extension of the model described in [Wyatt et al. \(2007a,b\)](#) to include delayed stirring by splitting disks into a series of concentric annuli. The implementation uses the equations in §2 of [Wyatt et al. \(2007a,b\)](#) and sums over 100 logarithmically spaced annuli to create a disk with radial extent. The self-stirring prescription is semi-empirical, based on the more detailed models of [Kenyon & Bromley \(2008\)](#) (see §3.1). Here, we briefly summarise the model and refer the reader to §2 of [Wyatt et al. \(2007a,b\)](#) for details omitted here.

We use a Minimum Mass Solar Nebula (MMSN, [Weidenschilling 1977](#)) surface density profile to specify the disk mass

$$\Sigma = \eta M_{\star} \Sigma_0 r^{-\delta}, \quad (2)$$

where η is a scaling parameter reflecting a range of disk masses, M_{\star} is in Solar units, radial distance r is in AU, and the surface density at 1 AU is $\Sigma_0 = 30 \text{ g cm}^{-2}$ ($1.1 M_{\oplus}/\text{AU}^2$ in our units). The power-law index δ is typically 1–1.5; we use 1.5 as our canonical value. This surface density provides roughly the amount of solid material contained in the outer Solar System. The surface density scales linearly with stellar mass, consistent with mm observations of protoplanetary disks. However, the range of stellar masses in our model is much smaller than the expected range of η , so the factor M_{\star} is relatively unimportant ([Natta et al. 2000](#); [Andrews & Williams 2005](#)). For extended disks the inner and outer radii are independent and specified by r_{in} and r_{out} . Narrow belts are specified by their radii r_{mid} and width dr (so for belts $r_{\text{in,out}} = r_{\text{mid}} \pm dr/2$).

Where [Wyatt et al. \(2007b\)](#) considered a range of total masses M_{tot} , we consider a log-normal distribution about η_{mid} .² There is as yet no evidence of a positive correlation between disk mass and radius (which might argue for the distribution of η to be narrower than that for M_{tot}), and thus we use the 1σ width of 1.14 dex observed for disk masses in Taurus ([Andrews & Williams 2005](#)).

The planetesimal disk is assumed to be in collisional equilibrium with a size distribution in each annulus defined by $N(D) = KD^{2-3q}$, where K is a constant, $q = 11/6$ for an infinite collisional cascade ([Dohnanyi 1969](#)), and D is planetesimal diameter. That distribution is assumed to hold from the largest planetesimal in the disk, of diameter D_c (in km), down to the size below which particles are blown out by radiation pressure as soon as they are created, D_{bl} (in μm). If q is in the range $5/3$ to 2 then most of the mass is in the largest planetesimals while the cross-sectional area σ_{tot} is dominated by the smallest particles:

² Previously each disk was assigned a total mass distributed about M_{mid} independent of disk location. This led to typical disks at $r = 120$ AU having about 6 times lower Σ_0 than disks at 3 AU (for $\delta = 3/2$). However, this difference is smaller than the dispersion in surface density and disk mass so is not particularly important.

$$\sigma_{\text{tot}} = 3.5 \times 10^{-17} K(3q - 5)^{-1} (10^{-9} D_{\text{bl}})^{5-3q} \quad (3)$$

in AU^2 .

We assume that particles act like blackbodies, so the fractional luminosity of grains $f = L_{\text{IR}}/L_{\star} = \sigma_{\text{tot}}/4\pi r^2$ for the annulus at r . The grain blowout size is

$$D_{\text{bl}} = 0.8 (L_{\star}/M_{\star}) (2700/\rho), \quad (4)$$

where D_{bl} is in μm , L_{\star} and M_{\star} are in Solar units, and density ρ is in kg m^{-3} . The dust temperature can be worked out from:

$$T = 278.3 L_{\star}^{0.25} r^{-0.5}. \quad (5)$$

We also assume that the central star acts like a blackbody.

Because we use a fixed size distribution with $q = 11/6$ in our model, the long-term evolution of the disk is determined by the removal of mass from the top end of the cascade. Planetesimals have a disruption threshold Q_{D}^* , and eccentricity e . The collisional lifetime of the largest planetesimals of size D_c at a radius r in an MMSN disk is

$$t_c = 2.2 \times 10^{-10} r^{23/6} D_c Q_{\text{D}}^{5/6} e^{-5/3} M_{\star}^{-7/3} \Sigma_0^{-1} \eta^{-1} \quad (6)$$

in Myr, obtained by substituting $\Sigma = M_{\text{tot}}/2\pi r dr$ into [Wyatt et al. \(2007b\)](#) Equation (9). We have simplified the relation here by assuming that $X_c = D_{\text{cc}}/D_c \ll 1$, where D_{cc} is the smallest planetesimal that has enough energy to catastrophically destroy a planetesimal of size D_c . This condition applies for the $e \gtrsim 0.01$ eccentricities found for self-stirring models ([Wyatt et al. 2007a](#)).

Assuming that collisions are the only process affecting the evolution of the surface density, then

$$\Sigma(r, t) = \begin{cases} \Sigma(r, 0) & t < t_{\text{stir}} \\ \Sigma(r, 0)/[1 + (t - t_{\text{stir}}(r))/t_c(r, 0)] & t > t_{\text{stir}} \end{cases} \quad (7)$$

where $\Sigma(0)$ is the initial surface density profile, t_{stir} is the delay until stirring (assumed to be 0 in [Wyatt et al. 2007b](#)), and $t_c(r, 0)$ is the collisional lifetime at r at that initial epoch. Where $t < t_{\text{stir}}$, the initial surface density profile applies.

Because more massive disks process their mass faster ($t_c \propto 1/\eta$), the surface density at late times ($t \gg t_c$ and $t > t_{\text{stir}}$) at a given radius is independent of initial surface density. Written in terms of the surface density of cross-sectional area in the disk (or simply “surface density” because $\tau_{\text{eff}} \propto \Sigma$, $\tau_{\text{eff}} = \sigma_{\text{tot}}/2\pi r dr = 2f r/dr$).

$$\begin{aligned} \tau_{\text{eff,max}} &= 1.2 \times 10^{-9} r^{7/3} D_c^{0.5} Q_{\text{D}}^{5/6} \\ &\times e^{-5/3} M_{\star}^{-5/6} L_{\star}^{-0.5} (t - t_{\text{stir}})^{-1} \end{aligned} \quad (8)$$

This prescription means that for a disk of known size at any given age, there is a maximum infrared luminosity, f_{max} , that can remain due to collisional processing. While f_{max} can be applied to unresolved stars based on the $24 - 70 \mu\text{m}$ colour and some assumption about disk extent ([Wyatt et al. 2007a](#)), $\tau_{\text{eff,max}}$ necessarily requires resolved observations for comparison. We return to the application of $\tau_{\text{eff,max}}$ to self-stirred disks in §3.3.

The final component of the model is the implementation of self-stirring, where successive annuli can be stirred at later times with increasing r (such as Eq. 1). Other

mechanisms for delayed-stirring, such as secular perturbations from an eccentric planet (e.g. [Mustill & Wyatt 2009](#)), can be implemented with different t_{stir} (see §5.1). The introduction of self-stirring also requires us to specify the level of disk emission before a disk is stirred. We assume that the emission is proportional to the surface density, but reduced by a factor x_{delay} with respect to that expected from Equation (3) because the collisional cascade has not yet begun. We estimate x_{delay} through comparison with the [Kenyon & Bromley \(2008\)](#) models below.

3 DEBRIS DISK EVOLUTION FOR INDIVIDUAL STARS

In this section we consider model evolution for individual disks, first making comparisons with the [Kenyon & Bromley \(2008\)](#) models, and then illustrating the surface density evolution. We then consider the implications for transience in the context of the [Wyatt et al. \(2007a\)](#) model and the effects of disk extent on excess evolution.

3.1 Comparison with [Kenyon & Bromley](#) models

We compare our model with the [Kenyon & Bromley](#) simulations of planet formation and debris disk evolution around A-stars to derive an empirical self-stirring time and x_{delay} that reproduces their excess evolution. Though [Kenyon & Bromley \(2008\)](#) derive relations for the time to reach the peak excess (their Eq. 55), and the radial time dependence for forming 1000 km objects (their Eq. 41), they do not derive a relation for the peak excess at different radial locations. Because our aim is to reproduce their excess evolution, we use the following empirical relation.

$$t_{\text{stir}} = 4 \times 10^{-4} r^3 \eta^{-1/2} M_{\star}^{-3/2} \quad (9)$$

in Myr. We first derived the numerical pre-factor and the exponent of η in this relation with a χ^2 minimisation procedure over models with $1.5 < M_{\star} < 3$ and $1/3 < \eta < 3$ at 24 and 70 μm . We fix the radial and stellar mass dependence because these are set by the orbital period and our assumption of $\Sigma \propto M_{\star}$. However, this formal method ignores some important model differences, in particular the continued stirring that appears to cause the [Kenyon & Bromley \(2008\)](#) models to decay faster at 70 μm (discussed below). We therefore arrive at Equation (9) by focusing on the 24 μm peak excesses. This different emphasis changes the values obtained in the formal fit at 24 μm by ~ 10 –20%.³

Though the dependence on η in Equation (9) is weaker than implied by Equation (1) ($-1/2$ vs. -1),

³ Similar variation is also found depending on how the [Kenyon & Bromley](#) models are weighted in the minimisation procedure. For example, lower weights for smaller excesses makes the peak excesses fit better, whereas constant weights fit the late time evolution better but underestimates the peak excesses. Allowing x_{delay} to vary results in values in the range ~ 0.01 –0.02.

the two should not necessarily agree. [Kenyon & Bromley \(2008\)](#) find that the time to peak dust production is $\propto \eta^{-1} M_{\star}^{-1.5}$ (as predicted by Eq. 1), but that the time to peak luminosity is $\propto \eta^{-2/3} M_{\star}^{-1}$ and takes much longer (their Eqs. 48 & 55). In comparing these proportionalities, it is important to remember that the peak dust production and peak luminosity are linked, but not directly. The observed luminosity depends on the history of the dust production rate and the rate at which small grains are being removed by radiation forces. Further, our empirical relation sets the evolution at specific r , rather than describing the global evolution of specific disk properties. Though Equation (9) is derived largely from the 24 μm evolution, we reproduce the f evolution, from which the [Kenyon & Bromley](#) peak luminosity is derived equally well. Our scaling of t_{stir} with η is probably weaker than their $-2/3$ because we set the *onset* of stirring, not the peak excess and higher mass disks reach their peak excess more rapidly once stirring starts (Fig. 1). We refer to the radial location where stirring has just begun (i.e. where $t = t_{\text{stir}}$) as r_{stir} .

Figure 1 shows a comparison of the [Kenyon & Bromley](#) model for an A2 ($2.5 M_{\odot}$) star with an equivalent one from our model. The 24 μm excess increases to a peak around 10 Myr, and then declines (see [Hernández et al. 2006](#); [Currie et al. 2008a](#); [Wyatt 2008](#); [Kenyon & Bromley 2008](#), for comparison with observations). In this example, the disk extends from 30–150 AU, and has $\eta = 1/3$, 1, and 3. We set the level of disk emission before stirring to $x_{\text{delay}} = 0.01$, which gives a reasonable match to the excesses prior to the formation of Pluto size objects. We take other model parameters from the best fit model of [Wyatt et al. \(2007b\)](#); $e = 0.05$, $D_c = 60$ km, and $Q_{\text{D}}^* = 150 \text{ J kg}^{-1}$. Though the largest objects in the disk are roughly Pluto size when the collisional cascade begins, [Kenyon & Bromley](#) find that objects larger than ~ 1 –10 km continue growing. Thus the effective maximum planetesimal size D_c for our model is of order 10 km because the smallest dust derives from a reservoir of objects of this size. Different choices for D_c , e , and Q_{D}^* change the rate at which excesses increase after the disk is stirred, though still give peak excesses that agree with the [Kenyon & Bromley](#) models within factors of a few.

To achieve the agreement shown in Figure 1 we must temporarily modify our model to match some [Kenyon & Bromley](#) assumptions about dust properties; they set $D_{\text{b1}} = 1 \mu\text{m}$, and use a “greybody” emission law $F_{\nu} \propto B_{\nu}(T) (1 - \exp(\lambda_0/\lambda))$ with $\lambda_0 = 10 \mu\text{m}$. They use [Yi et al. \(2001\)](#) luminosities, somewhat brighter than the [Schmidt-Kaler \(1982\)](#) luminosities used in our model. Finally, to ensure a good match between models we apply a factor 2.5 decrease to the [Kenyon & Bromley](#) excesses. The need for this factor is unsurprising considering the model differences and could, for example, arise from differences of a few percent in the average size distribution index q between D_c and D_{b1} . With these differences taken into account, both models produce fairly similar results. The delay in the rise of 24 and 70 μm excesses is similar, as are their magnitudes over the range A0–F2 (~ 1.5 – $3 M_{\odot}$) and $\eta = 1/3$ –3.

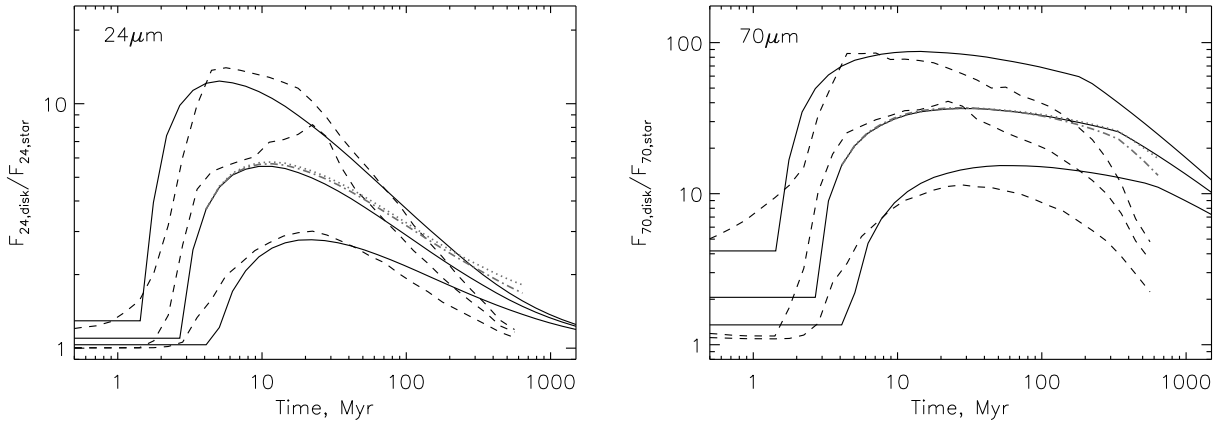


Figure 1. Evolution of $24\ \mu\text{m}$ (left) and $70\ \mu\text{m}$ (right) excesses for $\eta = 1/3, 1,$ and 3 for a disk from 30 to 150 AU from our model (solid lines) compared to models from [Kenyon & Bromley \(2008\)](#) (dashed lines), for an A2 ($2.5 M_{\odot}$) star. The main difference between the models at $70\ \mu\text{m}$ is caused by continued accretion and subsequent stirring in the [Kenyon & Bromley \(2008\)](#) models (see text). Also shown is the effect of the increasing main-sequence luminosity on an $\eta = 1$ disk with $D_{\text{bl}} = 1\ \mu\text{m}$ (grey dotted line) and then also allowing D_{bl} to vary (grey dot-dashed line). The overall effect of stellar evolution due to changing D_{bl} and hotter grains (i.e. dot-dashed line) is a small increase in $24\ \mu\text{m}$ excesses and a similar decrease in $70\ \mu\text{m}$ excesses.

The main difference is the decline in $70\ \mu\text{m}$ excesses at late times. Our model shows a fairly slow decline until after 200–600 Myr, when stirring reaches the outer disk edge and the excess decreases more rapidly because mass is being lost at all radii. The [Kenyon & Bromley \(2008\)](#) models show a faster decay. In their model, the largest objects continue to accrete once they reach Pluto size, thus increasing the rate of decay through removal of mass from the collisional cascade. More important is the increased stirring due to their continued growth, and the subsequent higher collision rates (S. Kenyon, *priv. communication*). This importance can be understood from the strong e dependence in Equation (6).

Figure 1 also shows the effect of including stellar evolution in our model (scaled to show relative differences). For fixed D_{bl} , increasing L_{\star} increases grain temperatures and the $24\ \mu\text{m}$ excess is higher. If D_{bl} is allowed to vary, the disk emission drops slightly due to smaller σ_{tot} as D_{bl} increases and the overall effect is a small increase in $24\ \mu\text{m}$ emission and a similar decrease at $70\ \mu\text{m}$.

After a few hundred Myr, the [Kenyon & Bromley](#) $70\ \mu\text{m}$ excesses also show a break towards faster decay. They attribute this decrease to stellar evolution as the star nears the end of its main-sequence lifetime (of 650 Myr for $2.5 M_{\odot}$). Higher stellar luminosity increases the importance of PR drag relative to collisions and the disk emission drops more rapidly as grains spiral toward the star. However, any mass lost to PR drag is probably due to the assumption of a fixed D_{bl} , as these models are of observable disks, which are generally not tenuous enough to suffer PR drag before grains collide ([Wyatt 2005](#)). For the A2 star in Figure 1, D_{bl} should increase from about 10 to $20\ \mu\text{m}$ during the MS lifetime, so fixing $D_{\text{bl}} = 1\ \mu\text{m}$ allows PR drag to remove grains that would have instead been blown out of the system. Also, a disk is unlikely to become PR dominated by realistic

increases in stellar luminosity.⁴ Our model shows a break at 200 Myr for the $\eta = 3$ (top) line at $70\ \mu\text{m}$ when stirring reaches the outer edge of the disk. Given that PR drag is unlikely to be the cause, the further drop in the [Kenyon & Bromley](#) models after ~ 200 Myr may in part be for the same reason.

In summary, we have shown that our simplified model is in good agreement with the [Kenyon & Bromley \(2008\)](#) models, with the main remaining discrepancies arising for older stars at $70\ \mu\text{m}$. The effect of changing main-sequence luminosities is small, and continued accretion by the largest bodies leads to smaller $70\ \mu\text{m}$ excesses after the peak is reached. We retain our prescription for D_{bl} , the main cause of the initial differences because it is well established that grains should respond to radiation forces (e.g. [Burns et al. 1979](#)). We allow x_{delay} to vary, though it is usually unimportant because most emission comes from stirred regions.

3.2 Evolution of surface brightness

Debris disks around some of the closest stars have been resolved, providing spatial information that cannot be derived from unresolved photometry. In this section we show disk profiles derived from our model for comparison. With delayed stirring there are two possible ways for the disk to evolve when stirring begins. These are set by the collisional (t_c) and stirring (t_{stir}) times. These two modes

⁴ For fixed M_{\star} and r the orbit decay timescale for smallest grains (which are most affected by PR drag) is $t_{\text{PR}} \propto D_{\text{bl}}/L_{\star}$. However, because D_{bl} increases with L_{\star} (Eq. 4), the PR timescale for the smallest grains is constant. The collisional lifetime of the smallest grains increases slowly as $t_{\text{coll}} \propto \sqrt{D_{\text{bl}}}$. For fixed $\beta = 0.5$, the relative importance of PR drag vs. collisions $\eta_0 \equiv t_{\text{PR}}/t_{\text{coll}} \propto 1/\sqrt{L_{\star}}$, and therefore changes little for the factor \sim few changes in main-sequence L_{\star} .

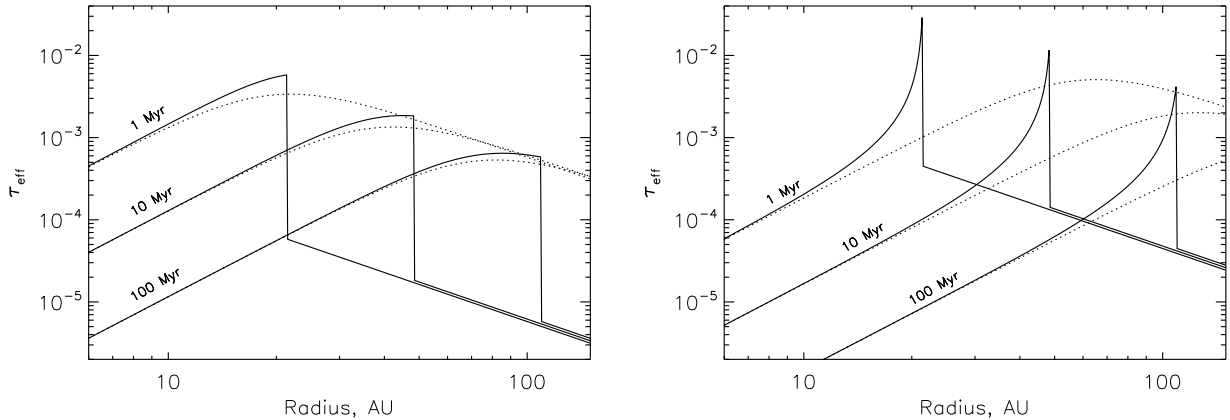


Figure 2. Evolution of τ_{eff} for self-stirred (*solid lines*) and pre-stirred (*dotted lines*) disks at 1, 10, and 100 Myr. In the left panel $t_c \gg t_{\text{stir}}$ so evolution is “slow” and similar to the pre-stirred case. In the right panel $t_c \ll t_{\text{stir}}$ so the evolution at r_{stir} is “fast” and much more violent as the disk reverts to the equilibrium state. Lines are offset slightly to remove ambiguities. The disks extend from 5–150 AU around an A2 star and have parameters: $\eta = 1$, $Q_D^* = 150 \text{ J kg}^{-1}$, $e = 0.05$, $x_{\text{delay}} = 0.01$, and $D_c = 60 \text{ km}$ (*left panel*) and $D_c = 1 \text{ km}$ (*right panel*). The peak surface density is larger for the fast self-stirred disk because more mass is concentrated in smaller size objects.

of evolution are shown in Figure 2, which shows the τ_{eff} evolution vs. radius in an extended disk at several times.

In Figure 2, we also compare the evolution with a pre-stirred disk—one that is stirred when the star is born at $t = 0$ (dotted lines). In this case the surface density profiles increase with radius to a broad peak. The slope of the inner region, where mass at all radii is being depleted collisionally, is set by $\tau_{\text{eff,max}} \propto r^{7/3}$ (Eq. 8). Outside the peak the primordial τ_{eff} remains because the collisional time is longer than the disk age there (i.e. $\tau_{\text{eff,max}} \propto r^{-3/2}$). The location of the peak moves outward with time ($r \propto t^{6/23}$, Eq. 6) as more distant regions begin to decay.

The solid curves in Figure 2 (left panel) show the self-stirred evolution when the collisional time is longer than the stirring time. Compared to the pre-stirred case, the difference is the x_{delay} drop outside r_{stir} where the disk has not been stirred and accretion is ongoing. For this disk little decay happens at r_{stir} immediately, but begins later when $t > t_c$. This evolution is therefore similar to the pre-stirred case, and we term this mode of evolution “slow” for a self-stirred disk. Compared to a pre-stirred disk, the factor x_{delay} leads to a narrower observed annulus if the disk is too faint to be detected outside r_{stir} . For comparison, see Figure 9a of [Kenyon & Bromley \(2004\)](#), which shows a qualitatively similar profile.

In the other limit, when the collisional time is shorter than the stirring time (Fig. 2, right panel), for a given age the disk at r_{stir} has much more mass than it would if it were pre-stirred (the same mass as at $t = 0$). The onset of stirring is therefore violent, with the rapid shedding of mass just inside r_{stir} as the disk reverts to its “equilibrium” state, that of a pre-stirred disk where the decay is independent of initial mass. This evolution was hinted at by [Dominik & Decin \(2003\)](#), where the excesses of disks with longer delay times decayed faster with time (their Fig. 3). We call this evolution the “fast” mode. These disks appear transient because the surface density can

be significantly above the expected pre-stirred level for their age (see §3.3).

However, we consider fast self-stirred disks with very sharp surface density profiles unlikely, because disks with short collisional times will start to decay before Pluto-size objects form. Planetesimal eccentricities increase as the largest objects grow, and t_c decreases accordingly. Thus, a disk that would stir in the fast mode in our model would in fact begin to decay earlier when $t > t_c$ (unless planetesimal eccentricities increase rapidly, in which case the time difference is small).⁵ Because the largest objects continue to grow after the disk is stirred, eccentricities continue to increase. After stirring, t_c continues to decrease until the disk begins to decay. Thus, we also do not expect disks where the stirring time is significantly shorter than the collisional time.

By equating the stirring and collisional timescales (Eqs. 9 & 6), we can derive the conditions required for the boundary between these regimes of evolution at r_{stir} (assuming $X_c \ll 1$). Evolution will be “slow” at r_{stir} if

$$\mathcal{R} \equiv r_{\text{stir}}^{5/6} D_c Q_D^{*5/6} e^{-5/3} M_*^{-5/6} \eta^{-1/2} > 2 \times 10^6. \quad (10)$$

At 50 AU on the 10 Myr curves, the disks illustrated in Figure 2 have $\mathcal{R} = 4 \times 10^6$ (left panel) and 6×10^4 (right panel), 2 times greater, and 33 times smaller than Condition (10) respectively. Because the collisional time increases more strongly with distance than the stirring time, inner disk regions are more prone to fast evolution, as are disks with weak or small planetesimals. There is some tendency towards fast evolution for more massive disks, though if the stirring time were simply the Pluto formation time (Eq. 1) this condition would be independent of surface density. Because disks with $\mathcal{R} \sim 10^6$ are the most physically plausible within our model, we check

⁵ In §5.1 we show that disks that evolve in the fast mode are possible if the stirring mechanism is secular perturbations from an eccentric planet.

the distribution of \mathcal{R} when generating population models in §4.

The evolution of slow self-stirred disks makes clear predictions for resolved observations of debris disks. While the brightest disks will yield broad surface density profiles, fainter disks only have an annulus of detectable emission because the surface density drops away interior and exterior to where the peak emission occurs. The observed width of the disk depends on how fast the disk is decaying relative to its age; however, we do not expect surface density profiles as sharp as shown in the right panel of Figure 2 for self-stirred disks. Of course, the disk extent is also set by where planetesimals can form and where they are not affected by external effects such as clearing, accretion, or ejection by planets.

For slow self-stirred disks the peak emission is set by the collisional time (i.e. the peak surface density in the left panel of Fig. 2 is slightly interior to r_{stir} at 100 Myr)

$$r \propto t^{6/23}. \quad (11)$$

If the difference between the level of emission at the peak and at r_{stir} is small (as in the left panel of Fig. 2 at 1 Myr), and the disk beyond r_{stir} is too faint to detect, then the outer edge of slow self-stirred disks will still appear to increase with time as $r \propto t^{1/3}$ (Eq. 9).

3.3 Transience

In the Wyatt et al. (2007a) model, narrow pre-stirred planetesimal belts have a maximum luminosity. This property arises because the decay time depends on the disk mass, and all disks were assumed to be stirred at $t = 0$. With an assumption about their width dr , the value f_{max} can be calculated for unresolved belts with observations in several bands, which gives an estimate of their radii. If the disk luminosity is significantly higher than f_{max} the excess is unlikely to arise from steady-state evolution.

Ideally, comparisons would be made between resolved disks and the predicted maximum surface density $\tau_{\text{eff,max}}$. As discussed above, we do not expect self-stirred disks to have τ_{eff} significantly greater than $\tau_{\text{eff,max}}$; those that do may be transient. However, because disks may be secularly stirred in the fast mode (§5.1), they can appear transient without being so in the sense meant by Wyatt et al. (2007a). Another issue, whether disks are extended or narrow belts is important because disks that are truly transient may not appear to be if they are assumed to be wider than they actually are. Therefore, if disks are narrow belts then f_{max} is a reasonable indicator of transience.

3.4 Radius evolution

There are considerable differences between the evolution of narrow belts and extended disks. Figure 3 shows the f vs. r_{24-70} evolution for disks extending from 15–120 AU for a range of initial surface densities, and a series of narrow belts with the same surface density centred at different r_{mid} between 20 and 70 AU (r_{24-70} is the radius

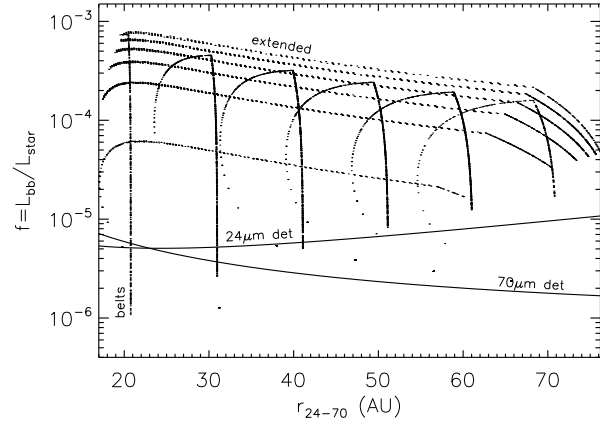


Figure 3. Evolution of narrow belts and extended disks (as labelled) in f vs. r_{24-70} space from 1 Myr to 1 Gyr. Disk r_{24-70} increases as stirring moves outward (so evolution is left to right). Here, f is derived from a blackbody at r_{24-70} (i.e. what detection at 24 and 70 μm would imply). Solid lines show 24 and 70 μm blackbody detection limits from Wyatt et al. (2007b). Extended disks have $r_{\text{in-out}} = 15\text{--}120$ AU and $\eta = 0.05\text{--}1.05$. For belts $r_{\text{mid}} = 20, 30, 40, 50, 60,$ and 70 AU, $dr = r_{\text{mid}}/2$, and $\eta = 1$. Belts increase in radius from left to right, and extended disks increase in f with higher η . Other model parameters are as in the left panel of Figure 2.

inferred from the 24 – 70 μm colour assuming blackbody grains at a single temperature, Eq. 5).

For extended disks r_{24-70} increases as r_{stir} moves outward. The disk r_{24-70} is located between the inner edge and where the surface density peaks, so moves outward with time. It is not simply at the peak surface density because the inner disk contribution to the SED is non-negligible when $\tau_{\text{eff}} \propto r^{7/3}$. Thus, for extended disks the increase in r_{24-70} with time is in fact slower than expected by Equation (11). The fractional excess decreases somewhat because the decay of emission interior to r_{stir} is stronger than the increased emission from newly stirred regions.

In contrast, belts show a small change in radius and then decay at near constant radius once stirred to the outer disk edge. The narrower disk extent means that r_{24-70} is nearer the peak excess. When stirring reaches the outer edge, all disks break to a faster decline in f because no new regions can be stirred. Because the peak surface density is still evolving outward (i.e. these disks are evolving in the slow mode), r_{24-70} continues to increase. When $t \gg t_c$ at the outer edge, f decreases at constant r_{24-70} (because the disk has $\tau_{\text{eff}} \propto r^{7/3}$ everywhere and r_{24-70} cannot change). Because the collision time scales more strongly with radius than stirring ($t_c \propto r^{23/6}$ vs. $t_{\text{stir}} \propto r^3$), most disks do not reach evolution at constant r_{24-70} until long after the outer disk edge is stirred (and long after the maximum 1 Gyr age shown in Figure 3). That is, slow evolution is more likely to occur at large radii (Eq. 10).

For comparison, pre-stirred disks show similar trends to Figure 3, but f can only decrease because pre-stirred disks start evolving at $t = 0$ everywhere. Thus, pre-stirred

disks do not show the initial increase in f seen for the self-stirred evolution. Also, there is no break to a faster decline in f , as occurs when self-stirring reaches the outer disk edge.

4 APPLICATION TO A-STAR STATISTICS

In this section we apply our model to evolution of 24 and 70 μm excesses around A-stars. We first outline the observations and the limitations of the pre-stirred model. Our aim is to test whether self-stirring can successfully reproduce the rise in 24 μm emission at ~ 10 –30 Myr (and the 24 and 70 μm statistics at other times), and see what constraints the statistics set on model parameters.

4.1 The A-star sample

The observations are compiled from several sources. Rieke et al. (2005) and Su et al. (2006) observed large unbiased samples of A-stars at 24 and 70 μm with *Spitzer*. While these samples provided the basis for the Wyatt et al. (2007b) study of pre-stirred evolution, they comprise stars mostly older than 10 Myr.

To supplement these data, we collect 24 μm data for B8–A9 stars in the following young clusters/associations: σ Ori (Hernández et al. 2007), OB1a/b (Hernández et al. 2006), λ Ori (Hernández et al. 2009), γ Velorum (Hernández et al. 2008), Upper Sco (Carpenter et al. 2009), β Pic Moving Group (BPMG Rebull et al. 2008),⁶ NGC 2232 (Currie et al. 2008b), and IC 2391 (Sieglar et al. 2007). We use the K_s –[24] excess to derive $F_{24,\text{disk}}/F_{24,\star}$ for these objects and use spectral types from Kharchenko (2001) where needed. These data make a sample of about 400 A-stars observed at 24 μm with ages between ~ 3 –800 Myr. All stellar photospheres in these samples are detectable and there are no upper limits (i.e. disk detections are calibration limited). We do not include stars in more distant regions, where observations are sensitivity limited and excess fractions are lower limits.

Because our 24 μm sample includes stars younger than 10 Myr old, it is possible that some are protoplanetary disks. However, consistently shorter disk lifetimes around intermediate mass stars mean that few A-star protoplanetary disks survive beyond a few Myr (Kennedy & Kenyon 2009). Indeed we exclude only three stars; V346 Ori in OB1a, HD 290543 in OB1b, and HD 245185 in λ Ori, which have K_s –[24] ≈ 6.5 –7.5 and strong IRAC excesses (Hernández et al. 2006). Less certain is whether the youngest stars in our sample contain dust left over from the protoplanetary disk phase, rather than from that created by fragmentation from self-stirring (e.g. Wyatt 2008).

Figure 4 (left panel) shows the 24 μm excesses as a function of time binned into “large” ($F_{24,\text{tot}}/F_{24,\star} >$

2), “medium” ($1.25 < F_{24,\text{tot}}/F_{24,\star} < 2$), and “small” ($F_{24,\text{tot}}/F_{24,\star} < 1.25$) excesses. The age bins are 0–6 Myr, 6–20 Myr, 20–40 Myr, 40–190 Myr, 190–400 Myr, and 400–800 Myr. There are 106, 45, 37, 130, 51, and 33 stars in these bins respectively. The primary result at 24 μm is a decline in excesses on a ~ 150 Myr timescale (Rieke et al. 2005).⁷ The large and medium excess bins add to give a peak in debris disk fraction at 30 Myr (e.g. Currie et al. 2008b). By separating the excesses into three bins, there is perhaps evidence for an additional trend: the large excesses peak around 10 Myr, and the medium excesses peak around 30 Myr. This behaviour suggests a population of large excess disks that form around 10 Myr, and then decay relatively rapidly to produce the medium excess population a few tens of Myr later.

Though these features are tantalising evidence of systematic trends that may be caused by self-stirring, their existence is motivated more by expectations than by statistical significance. In addition, Carpenter et al. (2009) note that because A-stars take ~ 10 Myr to reach the main-sequence, stars of fixed spectral type decrease in luminosity from 1–10 Myr. The decreasing luminosity decreases D_{bl} , and can cause at least some of the rise in 24 μm excesses that has been attributed to self-stirring. Using the cumulative distributions shown in Figure 4 (right panel) we estimate the significance of changes between different age bins with the KS test. According to this test, each pair of cumulative distributions for the three youngest bins (three upper curves) could have all come from the same distribution (max KS probability of difference is 82%). There is at least a 99% chance that all other combinations of distributions are not drawn from the same distribution, with the exception of the fourth age bin when compared to the fifth age bin (78%). That is, there is a robust decay in excesses from early to late times. For the individual clusters collected above, aside from the 50 Myr IC 2391, there is no pair different at more than the 98% level according to the KS test, though NGC 2232 is different from σ Ori, Orion OB1b, and γ Vel at 93–98%, and Upper Sco is different from the BPMG at 92%. Therefore, while there are interesting trends at early times, the only formally secure result is that 24 μm excesses decrease after ~ 50 Myr.

While there are far fewer observations of A-stars at 70 μm , we use the Su et al. (2006) stars, comprising 153 stars (including 19 observed with IRAS, and excluding Be stars HD 21362 & HD 58715 and Herbig Ae/Be star HD 58647). These data include many upper limits, which are largely for stars farther than 100 pc. For the model comparison undertaken here, we use the sample as given by Table 4 of Su et al. (2006) (shown in Fig. 9 of that paper, or Fig. 2 of Wyatt et al. (2007b)). As in Su et al. (2006) and Wyatt et al. (2007b), the data are binned into “large” ($F_{70,\text{tot}}/F_{70,\star} > 20$), “medium” ($5 < F_{70,\text{tot}}/F_{70,\star} < 20$), and “small” ($F_{70,\text{tot}}/F_{70,\star} < 5$)

⁶ β Pic is removed from the Rieke et al. (2005) sample. We set the excesses of the Be stars HD 21362 (Rieke sample), HD 67985 (γ Vel), and HIP 78207 (Upper Sco) to $F_{24,\text{tot}}/F_{24,\star} = 1$.

⁷ This decay is more obvious when viewed on a linear-time plot (e.g. Rieke et al. 2005; Su et al. 2006; Wyatt et al. 2007b) and is only seen in the oldest three bins in Figure 4.

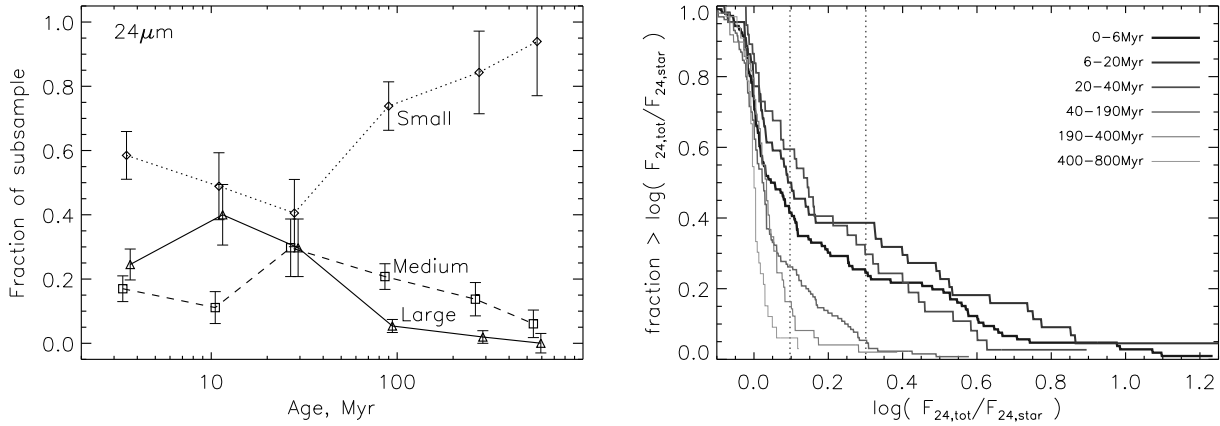


Figure 4. Evolution of A-star $24\mu\text{m}$ excesses. The left panel shows stars binned by age and large (triangles), medium (squares) and small (diamonds) excesses (ages offset slightly for clarity). Error bars are \sqrt{N} in each bin and for the oldest large excess bin we assume 1 disk to calculate the error. Excesses reach an overall peak around 30 Myr. The right panel shows cumulative distributions of $24\mu\text{m}$ excesses for the same age bins, from dark to light grey lines. The dotted lines indicate the bin edges for small, medium, and large excesses. In the second youngest bin HR4796A and β Pic are beyond the right edge of the plot.

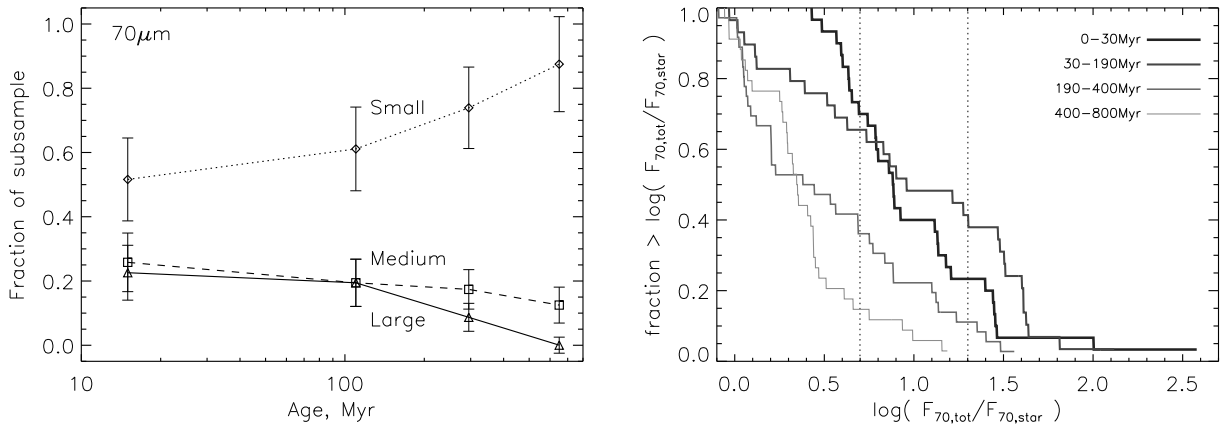


Figure 5. Same as Figure 4, but for $70\mu\text{m}$ excesses.

excesses. The data are also binned by age: 0–30 Myr, 30–190 Myr, 190–400 Myr, and 400–800 Myr.

The inclusion of upper limits in the $70\mu\text{m}$ sample means that the excess fractions are upper limits. As a check, we compare this sample to an unbiased subset of stars closer than 100 pc (and exclude IRAS sources, all but 2/19 of which are upper limits). In this subset only two stars (HD 27962 & HD 142703) with upper limits fall above the small excess bin (with $F_{70,\text{tot}}/F_{70,\star} < 5.61$ & < 7.63 respectively). The only significant difference between these two samples lies in the youngest age bin, where the <100 pc subset has only one star (of 11) with a small excess, compared to 16 (of 31) for the full sample. This difference arises because the main sample includes many Upper-Sco sources (~ 150 pc away) that have upper limits in the small excess bin. However, the paucity of young star forming regions within 100 pc also results in poor statistics in this bin (with only 11 stars). An alternative approach, setting all stars with upper limits to have small excesses, gives a $\sim 10\%$ increase in small excesses for the

youngest two age bins, and little difference for the older two. For both approaches, there is little change in the excess fractions in all but the youngest age bin (relative to Poisson errors). Based on these comparisons, we conclude that differences in the youngest age bin simply reflect poor statistics due to a lack of very close young stars. The small differences between (sub)samples in the older age bins mean that sample choice does not affect our results. Thus, we use the entire Su et al. (2006) $70\mu\text{m}$ sample for comparison with our model.

Figure 5 shows the evolution of excesses at $70\mu\text{m}$. As with the older age bins at $24\mu\text{m}$, these decay monotonically with time, but with a slower timescale of $\gtrsim 400$ Myr (Su et al. 2006). A KS test shows that the differences between adjacent age bins are not particularly strong (~ 90 – 98% chance of not being from the same distribution), but it is very unlikely that non-adjacent bins could be taken from the same distribution (with probabilities $>99.99\%$). Therefore, the decay from a higher to lower fraction of $70\mu\text{m}$ excesses over time is robust.

Finally, we use the [Wyatt et al. \(2007b\)](#) 46 star subsample of stars for which excess emission has been detected at both 24 and 70 μm by *Spitzer* (or 25 and 60 μm by *IRAS*). With the assumption of blackbody grains at a single temperature, this sample provides a set of disk radii (r_{24-70}) for comparison with our model.

4.2 Method

We now explore various population models and their ability to reproduce the A-star statistics. For these models, we select 30,000 stars randomly in the spectral type range B8–A9 with uniform $\log(\text{age})$, assuming all stars are born with planetesimal disks. As in [Wyatt et al. \(2007b\)](#) we fix some parameters and allow others to vary. We fix $\rho = 2700 \text{ g cm}^{-3}$, $q = 11/6$, $I = e$ and do not consider the effects of varying them. These assumptions leave Q_{D}^* , D_c , e , η , and the disk radii as parameters.

In addition to comparison of fractional excesses in different age bins, our modelling process also involves comparison of model and observed disk radius distributions using r_{24-70} .

The low significance of the 24 μm trends means that we measure the ability of the self-stirring model to fit A-star statistics at early times partly with a formal χ^2 measure for the 24 and 70 μm statistics and the r_{24-70} distribution, but also the success of the model at reproducing trends in the data. In some cases we can rule out models based purely on a poor fit to the statistics for the older A-stars, in which case our conclusions are independent of the low significance of trends for the younger stars.

4.3 Pre-stirred disks

To illustrate the shortcomings of the pre-stirred model for young stars, the best fit parameters from [Wyatt et al. \(2007b\)](#) are compared to the A-star observations in [Figure 6](#). This Figure uses the model of [§2](#) with $t_{\text{stir}} = 0$ so that disks are pre-stirred. The parameters are: $Q_{\text{D}}^* = 150 \text{ J kg}^{-1}$, $D_c = 60 \text{ km}$, $e = 0.05$, and a planetesimal belt radius distribution $N(r) \propto r^{-\gamma}$ with $\gamma = -0.8$ and disk width $dr = r_{\text{mid}}/2$. We find that $\eta_{\text{mid}} = 0.2$ gives the best results ([Wyatt et al.](#) specified the disk mass distribution with $M_{\text{mid}} = 10 M_{\oplus}$). The Figure shows that the model still reproduces the 24 and 70 μm A-star statistics for stars 100 Myr and older, but fails to reproduce the trend in large and overall excesses for younger stars at 24 μm . The model shows only a monotonic decline in the overall fraction of stars with excesses in contrast to the observations.

As a metric for comparing models, we quote the χ^2 value at 24 and 70 μm , for the distribution of radii r_{24-70} , and the sum of all three. These are computed as the sum of squared differences between the data and model divided by the Poisson error for all 18 data points at 24 μm (six age bins and three excess bins), 12 points at 70 μm (four age and three excess bins), and 5 points for the r_{24-70} distribution. In the pre-stirred case shown in [Figure 6](#), the values are $\chi_{24}^2 = 32.4$, $\chi_{70}^2 = 5.2$, and $\chi_r^2 = 17.0$, for a total of $\chi_{\text{tot}}^2 = 54.6$. Though these numbers give no

indication of why a particular model succeeds or fails, or whether it reproduces the desired trends, they formally show how well the statistics are reproduced and provide a benchmark for measuring the success of different self-stirring models.

4.4 Delayed stirring: the simplest case

By taking the peak in large excesses at 10 Myr as an indication of the delay time, we can add the simplest possible model of delayed stirring to our model. [Figure 7](#) shows a model with almost the same parameters as the pre-stirred model with the addition of a 10 Myr delay (1σ width 0.1 dex) before the onset of stirring for all disks (here $\eta_{\text{mid}} = 0.25$). After this delay all disks begin evolving, regardless of radius. This simple modification to the model reproduces the 24 μm excesses better than the pre-stirred model with some change at 70 μm , yielding $\chi_{24}^2 = 19.9$, $\chi_{70}^2 = 12.5$, and $\chi_r^2 = 21.9$ for a total of $\chi_{\text{tot}}^2 = 54.3$. The three 24 μm excess bins now show the right general trends: the large excesses peak at 10 Myr, the medium excesses show a broad peak over 10–100 Myr, and the small excesses reach a minimum around 10–30 Myr. The fraction of small 70 μm excesses at the earliest times increases due to more unstirred disks. An obvious physical motivation for this prescription is unclear, though there are some possibilities that may merit further study.

One possibility might seem to be objects emerging from a protoplanetary disk phase somewhat longer than the “typical” 6 Myr lifetime (e.g. [Haisch et al. 2001](#)). However, this explanation is unlikely for two reasons. Primarily, only a small fraction of stars have long lived disks, not the $\sim 40\%$ suggested by [Figure 4](#). Further, primordial disk lifetimes around A-stars are consistently shorter than for less massive stars ([Kennedy & Kenyon 2009](#)). Therefore, the delay between primordial disk dispersal and the creation of large 24 μm excesses is too long for a plausible direct link.

A possible delay mechanism is scattering of proto-planets and embryos to unstirred locations in the outer disk, where they stir smaller objects to collision velocities. In this scenario the same fraction as in the 10 Myr peak, $\sim 40\%$, of stars must harbour planets that undergo scattering events. This figure is higher than the fractions of intermediate mass stars both known (9% for 1.3–1.9 M_{\odot} , [Johnson et al. 2007](#)) and predicted ($\sim 20\%$ for 2–3 M_{\odot} , [Kennedy & Kenyon 2008](#)) to have gas giants. However, stellar systems may contain many more undetectable lower mass and/or more distant planets so the fraction of stars with planetary systems is probably not a major problem for this scenario.

The main issues with a scattering scenario are timing and depletion. For all scattering events to occur at around 10 Myr seems to produce a fine tuning problem, when simulations of scattering around Solar-type stars show that instabilities can happen at a wide range of epochs. For example, in the case of the “Nice” model for the Late Heavy Bombardment (LHB) in the Solar System, [Gomes et al. \(2005\)](#) show that the LHB epoch varies strongly with the primordial Kuiper Belt’s inner edge location. In addition, this type of simulation is very

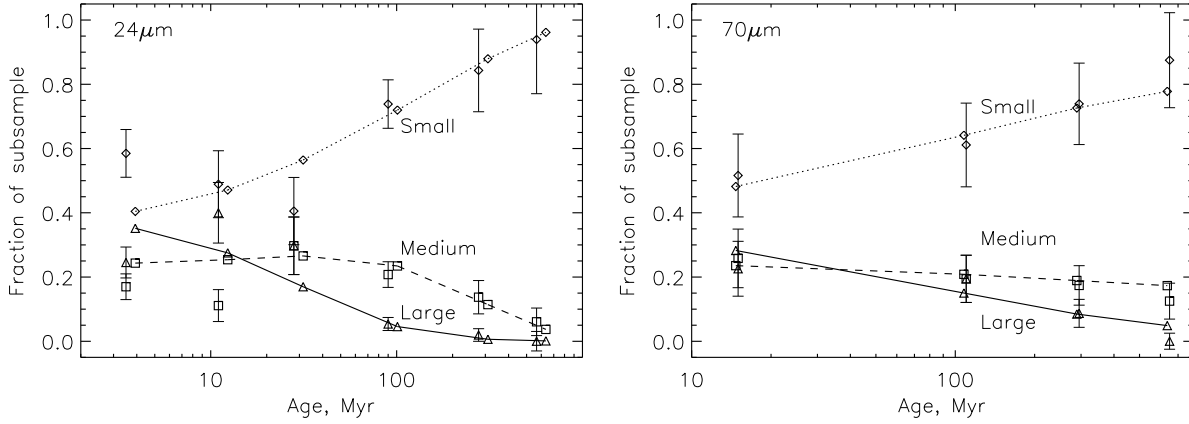


Figure 6. Best fit parameters for the Wyatt et al. (2007b) pre-stirred model at 24 and 70 μm (same symbols as Figure 4, joined by solid, dashed, and dotted lines for large, medium, and small excesses respectively). Symbols with error bars show observed A-star statistics. At 24 μm the model predicts too many stars with large excesses at the earliest times, and a monotonic decline in the overall fraction of stars with excesses. There are no new 70 μm data so the right panel is the same as Wyatt et al. (2007b) Figure 2.

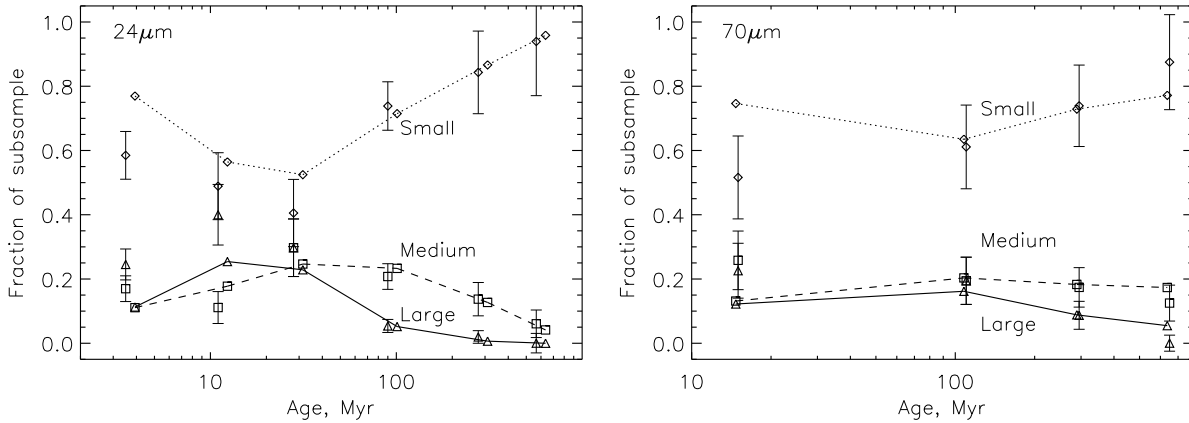


Figure 7. Simple delayed stirring model compared with 24 and 70 μm statistics. Symbols and lines are as in Figure 6. All disks begin their evolution after ~ 10 Myr.

sensitive to the initial conditions and it is unlikely that all systems undergo instability at any particular time.

The way that planetesimal belts are depleted during scattering events also presents a problem. Based on an analysis of the Nice model, Booth et al. (2009) show that the signature of an LHB like event is a drop in 24 and 70 μm excess ratios of around 4 orders of magnitude with a brief (~ 15 Myr) peak in 24 μm excess, meaning that excess fractions should drop, not peak when LHBs occur. Therefore, planet-planet scattering is an unlikely source of the trends seen in the 24 μm A-star statistics.

Another delay mechanism arises if planetesimals are initially large (“born big”, Morbidelli et al. 2009). The lack of an initial population of small grains means that observable dust is not generated until the large planetesimals collide and begin to decay, thus causing a rise and subsequent fall in the small dust population. This delay could plausibly be 10–30 Myr depending on the planetesimal properties and locations.

4.5 Self-stirring

We now turn to the self-stirring model. As discussed in §3.1, D_c is of order 10 km. The eccentricity when 1000 km objects form in the Kenyon & Bromley models is roughly constant with radius, and around $e = 0.01$. We therefore use these numbers as a order of magnitude guide and attempt to reproduce the A-star statistics with similar values. The remaining model parameters are Q_D^* , η_{mid} , and the disk radii. For self-stirring, x_{delay} has little impact on the results (see §3.2). Of particular importance is the inner hole specified by r_{in} (or the minimum r_{mid} for narrow belts), needed to ensure a peak in the overall fraction of stars with disks.

We consider two types of disks in our population models. These disks are motivated by observations that show debris disks are commonly narrow belts, in contrast to the structure of protoplanetary disks that extend from several stellar radii to hundreds of AU. Though resolved observations may not discern between a truly narrow belt

and an annulus of bright emission in an extended disk, Figure 3 shows that the excesses for these disks evolve quite differently. Comparing population models to the A-star statistics may therefore suggest which kind of disk is more common. Because protoplanetary disks are the precursors of debris disks, knowing whether they have the same spatial extent will yield information about likely mechanisms and locations for planetesimal and planet formation.

4.5.1 Narrow Belts

Figure 8 shows the model that best reproduces the A-star trends for narrow belts. Belt radii are taken from a distribution with $r_{\text{mid}} = 15\text{--}120$ AU and $\gamma = -0.8$. Belts have width $dr = r_{\text{mid}}/2$, $Q_{\text{D}}^* = 45 \text{ J kg}^{-1}$, and $\eta_{\text{mid}} = 0.15$. We set $D_{\text{c}} = 10$ km and $e = 0.025$, which are similar to the values expected from the [Kenyon & Bromley \(2008\)](#) models. The fit has improved significance over the pre-stirred and simple delay models with $\chi_{24}^2 = 22.4$, $\chi_{70}^2 = 15.0$, $\chi_{\text{r}}^2 = 2.1$ and $\chi_{\text{tot}}^2 = 39.5$.

Initially we expected that the 10–30 Myr delay for the rise in excesses would lead directly to an inner disk radius using Equation (9) for t_{stir} . Therefore, with $\eta \sim 0.15$ we expect $r_{\text{mid,min}} \sim 30$ AU for stirring to occur around 10 Myr (Eq. 9). However, setting $r_{\text{mid,min}}$ to values larger than ≈ 15 AU means that fewer disks are concentrated at small radii, and the distribution of inferred radii and the 70 μm excesses become inconsistent with the observations (see §4.6). Because we cannot simultaneously reproduce the statistics and have a peak in large excesses at 10 Myr, it is actually the 70 μm excesses and $r_{24\text{--}70}$ distribution that sets $r_{\text{mid,min}}$. The timing of the medium excess peak is partly set by Q_{D}^* because many of these disks decay from younger large excess disks. The relative fractions in the excess bins are set by the distribution of surface densities.

Though a reasonable fit to the 24 and 70 μm statistics and overall distribution of radii is possible, there is some difference in the distribution of radii with time (Fig. 8, lower right). At 100 Myr, the lower envelope of model disk radii starts to increase from 15 AU to ~ 60 AU by 800 Myr. This change is caused by the decay of smaller disks below detectable levels. Seven disks lie well away from the region populated by the model. The most discrepant disks are the same six noted by [Wyatt et al. \(2007b\)](#) when compared to the pre-stirred population model. All disks with radii less than 10 AU have $f/f_{\text{max}} > 20$ and may therefore be transient (HDs 38678, 115892, 3003, and 172555). The potential influence of PR drag was offered as an explanation for the remaining two, HD 2262 and HD 106591, which we maintain here and also apply to HD 97633.

As discussed in §3.2, we expect self-stirred debris disks to have stirring times similar to their collisional times (i.e. $\mathcal{R} \sim 10^6$). For the narrow belt model we find that the \mathcal{R} distribution peaks around 2×10^6 with nearly all disks within ± 1 dex.

In summary, we find a reasonable fit to the A-star statistics for self-stirred planetesimal belts with physically plausible parameters. The model does not show a

strong peak in large 24 μm excesses at 10 Myr because the disk masses and minimum belt radii required mean that many of the smallest disks are stirred at their inner edges before they are observed. However, the model does reproduce all A-star statistics and trends at both 24 μm and 70 μm .

4.5.2 Extended disks

We consider three possible populations of extended disks, loosely motivated by potential processes that may shape protoplanetary and debris disks: (1) Disks with some fixed inner hole size of a few tens of AU that extend to some variable outer radius, perhaps due to their natural size or truncation by stellar encounters or companions, (2) disks with a fixed outer radius and a variable inner hole size, perhaps cleared by planets that form at various locations, and (3) disks with fixed inner and outer radii, similar in structure to young protoplanetary disks. We do not consider disks with both variable r_{in} and r_{out} because these are effectively a mix of belts and extended disks and provide little useful information about which type of disk is more likely. We again use $D_{\text{c}} = 10$ km, and $e = 0.01$ as a starting point. When it is fixed, we set $r_{\text{out}} = 150$ AU. The variable inner or outer radii are chosen from a power-law distribution between the maximum and minimum with power law index γ .

For the most extended disks, those with fixed r_{in} and r_{out} , a reasonable fit to the 24 μm statistics can be found with r_{in} around 40 AU ($\chi_{24}^2 \sim 35$), but the 70 μm statistics and radius distributions are significantly different ($\chi_{70}^2 \sim 190$ and $\chi_{\text{r}}^2 = 50$). Similarly, for variable r_{in} with $\gamma = -0.8$ and fixed r_{out} , good fits to the 24 μm statistics ($\chi_{24}^2 \approx 30$) and radius distribution ($\chi_{\text{r}}^2 \approx 5$) can be achieved, but at the cost of a poor fit to the 70 μm statistics ($\chi_{70}^2 \sim 120$). The high χ_{70}^2 in both cases is due to $\sim 40\text{--}50\%$ of the model population having medium 70 μm excesses at late (>300 Myr) times.

This high fraction can be understood by looking at how extended disks evolve, shown in Figures 1 and 3. While the 24 μm excess declines as stirring moves further out in the disk, 70 μm excesses for extended disks only show small decreases while the disk is still being stirred. The $\eta = 1/3$ disk in Figure 1 (middle solid curves) has a 24 μm excess >2 between 7–100 Myr, and would thus contribute to the large 24 μm excess peak in the population model. The 70 μm excess for the same disk rises above the medium excess ratio of 5 at 6 Myr, and remains higher until after 1 Gyr. Even when stirring reaches the outer disk edge, the strong radial dependence on the collisional time means that at ~ 100 AU the excess only decreases slowly. Therefore, extended disks with fixed r_{out} that have large 24 μm excesses at early times have medium (or large) 70 μm excesses for long periods of time. This evolution means that the A-star statistics rule out self-stirred extended disks with fixed outer radii that evolve like our model. This conclusion is independent of the significance of the 24 μm trends for the younger A-stars.

Though fixed r_{out} leads to problems with the 70 μm excesses at late times, this issue can be addressed by allowing r_{out} to vary. With fixed $r_{\text{in}} = 15$ AU and the distri-

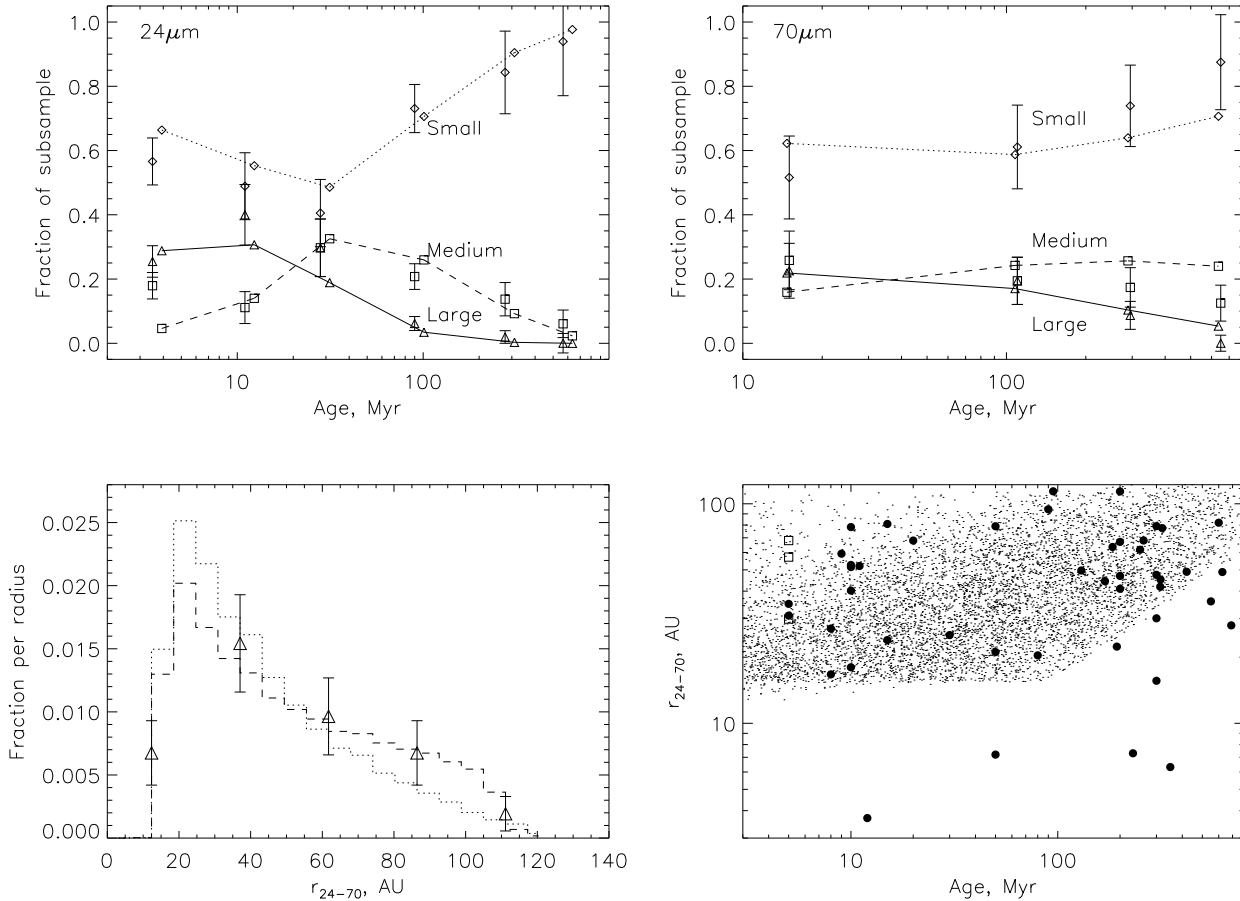


Figure 8. Best fit of the model population to 24 and 70 μm statistics with narrow belts. *Top left and right panels:* binned 24 μm and 70 μm evolution, *Lower left panel:* overall (dashed line) and detectable (dotted line) model r_{24-70} (omitting the four possibly transient sources noted in the text), and *Lower right panel:* r_{24-70} vs. t compared to the 46 star subsample (open squares show three additional sources detected by [Carpenter et al. 2009](#), HIP 76310, HIP 77911, and HIP 80088).

bution of r_{out} set with $\gamma = -0.8$, the 70 μm statistics can be reasonably reproduced ($\chi^2_{70} \sim 6$). However, this radius distribution has trouble reproducing the 24 μm statistics ($\chi^2_{24} \approx 100$) and the r_{24-70} distribution for the 46 star subsample, predicting too many disks with small radii ($\chi^2_r \approx 13$). Attempts to remedy this problem by increasing the number of wider disks (increasing the power law index γ) results in essentially fixing r_{out} , which leads to the previous problem of too many medium excess disks at 70 μm at late times. Thus, extended disks with fixed r_{in} also have trouble reproducing the A-star statistics.

The conclusion that extended disks cannot reproduce the A-star statistics may depend on the particular simplifying assumptions needed to make an analytic population model. A possible key difference is illustrated by [Figure 1](#): the [Kenyon & Bromley \(2008\)](#) models decay at 70 μm more rapidly than ours and the excesses are ~ 2 – 5 times lower after 100 Myr, probably due to continued accretion and stirring (see [§3.1](#)).

Whether continued accretion and stirring will lower the predicted 70 μm excesses for extended disks at late times without making the radius distribution significantly steeper (i.e. more disks at large r being undetectable) is not clear, but the comparison in [§5.2.1](#) of

[Kenyon & Bromley \(2009\)](#) gives some indication. Their model predictions of 70 μm excess fractions for disks with fixed r_{in} and r_{out} are several times higher than the [Su et al. \(2006\)](#) observations at the latest times, as we found in [§4.5.2](#). Therefore, it appears that extended disk models that include continued accretion and stirring still evolve too slowly at 70 μm , providing further evidence for the belt-like nature of debris disks.

4.5.3 Summary

Our population model suggests that debris disks are more likely to be narrow belts than extended disks. The formal χ^2 for narrow belts is an improvement over the pre-stirred model, and reproduces all A-star statistics, including the rise and fall in 24 μm excesses. The inability of extended disks to reproduce the statistics is due to how they evolve. Disks with fixed r_{in} predict too many disks at small radii and disks with fixed r_{out} predict too many 70 μm medium excess disks at late times.

The reason belts work well appears to be because they restrict the evolution of excesses. The power-law distribution of r_{mid} means that most disks are at rela-

tively small r , and the evolution is truncated when stirring reaches the outer edge (see Fig. 3). The r_{24-70} distribution is therefore a closer reflection of the initial power-law distribution, rather than being set by self-stirred disk evolution as for extended disks.

4.6 Constraints on the best fitting model

With the self-stirring model we have somewhat more power to constrain parameters than the Wyatt et al. (2007b) pre-stirred model. This ability arises because we have estimates of D_c and e based on the Kenyon & Bromley (2008) results. The remaining parameters left to fit the statistics are Q_D^* , η_{mid} , and the disk radii parameters $r_{\text{mid},\text{min}}$ and γ .

For the belt model surface density, we find $\eta_{\text{mid}} = 0.15$ gives the best fit. Because we find that debris disks tend to be belts, our use of a surface density law has only a minor impact on our model. There is a factor 5 difference in surface density from inner to outer disk edges, much smaller than the range of η we consider. Consequently, the model does not strongly constrain the initial surface density power-law index δ . For our best fit model we use $\delta = 1.5$, but find that populations with $\delta = 1$ produce similar results.

We find $Q_D^* = 45 \text{ J kg}^{-1}$ gives the best fit to the peak in medium $24 \mu\text{m}$ excesses, similar to that used for the comparison in §3.1. This value is best considered an effective value for the evolution, since a range of Q_D^* are expected for different size planetesimals and at different radii. Our Q_D^* is reasonable for weak rock and ice for $D \sim 10 \text{ km}$ for the $\sim 100\text{--}1000 \text{ m s}^{-1}$ range of collision velocities (Leinhardt & Stewart 2009). The value of 45 J kg^{-1} is a third of that found for the best fit model in (Wyatt et al. 2007b), but as in that paper Q_D^* and e are degenerate. Thus, our results do not change if $Q_D^*{}^{5/6} e^{-5/3} \approx 11100$. Löhne et al. (2008) show that the assumption of a single planetesimal strength is within an order of magnitude of a more complex model that includes a size-dependent planetesimal strength (their Fig. 11), with the largest differences occurring at late times $\gtrsim 1 \text{ Gyr}$.

Constraining the range of disk radii within the narrow belt model is also possible to some degree. The model has trouble producing a stronger peak in large excesses at 10 Myr while retaining a reasonable fit to the statistics. The model shows a slightly stronger peak in large excesses at $24 \mu\text{m}$ when the minimum r_{mid} is increased to 20 AU, but the fit to the $70 \mu\text{m}$ excess fractions becomes worse because the relative fraction of wider disks increases (for fixed γ). Therefore, at late times there are more disks with medium $70 \mu\text{m}$ excesses, essentially the same problem faced for extended disks with fixed r_{out} . We find it difficult to fit the A-star statistics with $r_{\text{mid},\text{min}} \gtrsim 20 \text{ AU}$ (where $\chi_{24}^2 = 32.5$, $\chi_{70}^2 = 24.8$, $\chi_r^2 = 5.2$ and total $\chi_{\text{tot}}^2 = 62.5$).

On the other hand, decreasing the inner hole size actually better the formal significance of the model fit to the A-stars. With $r_{\text{mid}} = 3\text{--}120 \text{ AU}$ and $\eta = 0.45$ we find $\chi_{24}^2 = 14.0$, $\chi_{70}^2 = 6.6$, $\chi_r^2 = 10.6$ and $\chi_{\text{tot}}^2 = 31.2$. This model shows a monotonic decline in excesses as

for the pre-stirred model. However, in contrast to our favoured belt model, this model predicts a population of disks younger than 100 Myr with r_{24-70} less than 15 AU. This region is empty in the lower right panel of Figure 8 (though we ignore disks we deem to be transient). Thus, while the typical minimum belt radius could lie between 3–15 AU, we favour the model with minimum belt radii $\approx 15 \text{ AU}$.

The power-law distribution of disk radii is fairly well constrained to $\gamma \approx -0.8$. This constraint arises due to the belt-like nature of disks, which means that the model γ must be similar to the observed distribution.

The chosen age distribution has a small effect on the large excess peak at 10 Myr. If we set the minimum age to 1 Myr (instead of 3 Myr based on σ Ori stars) then the peak becomes slightly stronger. The difference arises because including younger stars results in more unstirred disks (with small excesses) in the youngest age bin. Though this effect is minor, it shows that uncertainty in stellar ages can affect the results of the population model.

5 DISCUSSION

In the previous sections we have shown how self-stirred debris disks evolve. The model makes predictions, some of which can be compared to photometric observations, such as how disk radii inferred from blackbody models are distributed and evolve.

The most basic prediction of this kind for pre- and self-stirred models is that the radial location of peak emission should increase with time (Fig. 2). However, most surveys have failed to find any evidence for this trend (e.g. Su et al. 2006; Najita & Williams 2005). Rhee et al. (2007) find an apparent increase in disk radii inferred from IRAS colours. Unfortunately, all sources with disk radii greater than 100 AU—old stars largely responsible for the trend—have yet to be confirmed with new observations (i.e. with *Spitzer*). This picture is also complicated by the expected increase in the lower envelope of radii at late times as close-in disks drop below detection limits (Fig. 8 lower right; Wyatt et al. 2007b). Therefore, our model shows that the expected increase in radii may not be as obvious as predicted by Equation (11), and that other predictions of self-stirring could be more useful. For example, another prediction of self-stirring is that disks with large radii for their age should have higher than average disk surface density, because these disks stir to large radii the fastest.

However, it is important that these predicted trends are not just compared with photometric observations, because disk models based solely on SEDs can be degenerate and/or uncertain. Resolved imaging is necessary to confirm or correct SED-derived estimates. Imaging is also needed to test predictions such as the surface density profiles shown in §3.2. Below we take a detailed look at a subset of resolved debris disks with the aim of comparing observed disk characteristics with those predicted by models.

Also, we have not addressed an alternative possibility to self-stirring, that disks are stirred by secular

perturbations from planets not co-located with the disk (Mustill & Wyatt 2009). In this section we show that a model with t_{stir} set by planet-stirring can reproduce the A-star statistics and suggest that these planets could cause debris disks to be narrow belts. Because both mechanisms can fit the A-star statistics, high resolution imaging is the best way to differentiate between self-stirring and planet-stirring.

5.1 Self-stirring vs. planet stirring

The fact that the A-star observations are well reproduced with a self-stirring model shows that this mechanism may be important for debris disks. However, self-stirring is not needed as an explanation for systems such as β Pic where a planet is the likely stirrer. It is therefore important to predict features that allow the stirring mechanism to be identified. In the case of individual systems influenced by planets these features are well known, and stem largely from the same influence that causes planetesimal random velocities to increase and collisions to be destructive. Secular perturbations both warp the disk (e.g. β Pic) and cause it to be offset from the star (e.g. Fomalhaut). These features may be imaged directly, or an offset inferred from peri/apocenter glow (e.g. Wyatt et al. 1999). On shorter timescales, objects on unstable orbits too close to planets are ejected, which can result in sharp disk edges (e.g. Fomalhaut). The remaining way of identifying whether a planet may be the stirrer is to detect it directly (e.g. Fomalhaut, and perhaps β Pic).

Though these features provide a way of inferring a stirring mechanism (and discovering planets), they can only be applied to individual systems. Distinguishing the dominant stirring mechanism at a population level is more difficult, because planet-stirring introduces yet more parameters to the model. To briefly look at whether a planet-stirred population model can reproduce the A-star statistics, we use the stirring time assuming internal perturbers (Mustill & Wyatt 2009)

$$t_{\text{stir}} = 5 \times 10^{-5} \frac{(1 - e_{\text{pl}}^2)^{3/2}}{e_{\text{pl}}} \frac{r^{9/2} \sqrt{M_{\star}}}{M_{\text{pl,Jup}} r_{\text{pl}}^3} \quad (12)$$

in Myr, where the ‘pl’ subscripts indicate planet properties and r is the disk location where the stirring time applies.

The increased number of parameters allows more flexibility in reproducing the observed A-star statistics. For example, the A-star statistics can be reproduced as well as in Figure 8 for narrow belts if we set the stirring time with planet properties: $M_{\text{pl}} = 0.5 M_{\text{Jup}}$, $e_{\text{pl}} = 0.1$, $r_{\text{pl}} = r_{\text{mid}}/3$. That is, each belt is assumed to have a $0.5 M_{\text{Jup}}$ planet with eccentricity 0.1 located at one third of its average radius.⁸ We assume that planets form early—during the protoplanetary disk phase—so the formation time can be ignored. For comparison with the previous models, this planet stirred model has $\chi_{24}^2 = 19.7$,

⁸ Setting Equations (9) and (12) equal and solving for r_{pl} suggests $r_{\text{pl}} \propto \sqrt{r_{\text{mid}}}$. However, the stronger scaling may be needed to account for the stirring time being independent of disk mass.

$\chi_{70}^2 = 7.3$, $\chi_{\text{r}}^2 = 4.4$ and $\chi_{\text{tot}}^2 = 31.3$. This example is unlikely to be the only type of planet distribution that reproduces the observations, and shows that distinguishing between self-stirring and planet-stirring is not yet possible by this method. Future studies of this type can use distributions of known exoplanet properties as input, though these are only complete to ~ 5 AU, and disks may be perturbed by planets at much larger radii (e.g. Fomalhaut).

Some other interesting points can be made if disks are stirred by planets. The decreasing upper envelope of $24 \mu\text{m}$ excesses for A-stars suggests that the stirrers are not too far interior (or exterior) to the disk, because the strong radial dependence on the stirring time means that disks far from their planets will be unstirred early and then luminous at late times. This conclusion explains the success of the above example, where the planet location scales with the disk radius.

Because the stirring time is set by planet properties and not the disk mass, disks can stir in the fast mode and no longer have a maximum surface density $\tau_{\text{eff,max}}$ (see §3.2). Neighbouring planetesimal orbits can begin to cross at non-zero eccentricity as they precess, so the collision velocity steps from zero to the forced eccentricity times the Keplerian velocity when the disk is stirred (Mustill & Wyatt 2009). We can also derive a condition similar to (10), but now using Equation (12) for the stirring time. For an interior planet-stirred disk to evolve in the slow mode:

$$\mathcal{R}_{\text{pl}} \equiv \frac{e_{\text{pl}}}{(1 - e_{\text{pl}}^2)^{3/2}} r_{\text{pl}}^3 M_{\text{pl,Jup}} r_{\text{stir}}^{-2/3} M_{\star}^{-17/6} \times D_{\text{c}} Q_{\text{D}}^{\star 5/6} e^{-5/3} \eta^{-1} > 2.3 \times 10^5. \quad (13)$$

This relation is qualitatively different to Condition (10), because the planet-stirring time increases more strongly with radius than the decay time (see Fig. 6 of Mustill & Wyatt 2009). Thus, disks are more likely to evolve in the fast mode at large radii, because the disk is stirred so late that it would have decayed earlier if it were pre-stirred. Parameters that shorten the planet-stirring time, such as higher e_{pl} or M_{pl} , or larger r_{pl} (bringing the planet closer to the disk because this example is for interior planets) make the disk more likely to stir in the slow mode.

In summary, a population model of disks stirred by secular perturbations from planets can reproduce the A-star statistics if the planets are located near the disk. This model is unlikely to be unique, as different distributions of planet properties can probably give similar results. Therefore, it is not possible to distinguish between self-stirring and planet-stirring for debris disk populations by this method yet. The features shown by high resolution imaging of individual objects, such as warps and offsets, remain the best marker of debris disks influenced by planets. Our planet-stirred example also motivates planetary system architecture as a possible reason for debris disks to be narrow belts.

5.2 The origin of narrow belts

Returning to the idea that resolved disks can be roughly split into extended disks and belts (Kalas et al. 2006), our results suggest that debris disks tend to be narrow belts that have minimum radii of ~ 15 AU. A similar conclusion was reached by Chen et al. (2006), who found that most of their objects' IRS spectra were best fit by single temperature blackbodies colder than 130 K (thus also suggesting that disks have inner holes). In contrast, nearly all young stars have evidence for protoplanetary dust and gas disks that extend from very near the star (e.g. Haisch et al. 2001) to hundreds of AU (e.g. McCaughrean & O'dell 1996; Watson et al. 2007). The implication is that not only the primordial disk extent sets where debris disks reside, but other influences such as photoevaporation, disk fragmentation, and truncation and clearing by planetary and stellar companions. Within the context of the previous section, planets that stir the disk may also be responsible for clearing it at other locations. As is likely the case with β Pic (Augereau et al. 2001), apparently extended disks may result from the blowout of small grains created in a relatively narrow planetesimal belt.

To produce debris disks that are narrow belts, these mechanisms need to plausibly reproduce two qualitative trends: (1) disk inner and outer radii are positively correlated because we find that they are narrow belts, and (2) most disks have relatively small radii, to reproduce the observed power-law distribution of disk radii.

One possibility is that the belts are locations where planetesimal formation was possible or favoured. For example, one process that both clears dust from inner regions and enhances more distant regions is the influence of photoevaporative disk clearing. Alexander & Armitage (2007) show that after the inner gas disk has cleared, small grains ($\lesssim 10$ – 100 cm) are dragged outward as the inner edge of the gas disk moves outward. At some point, the gas disk either becomes too tenuous to keep moving the grains, or the dust density becomes comparable to the gas density. Either way, a concentrated mass of grains is left behind by the gas (though objects larger than ~ 1 m are less affected by this process). Formation of Pluto-size objects will be enhanced here, either simply due to the faster growth time, or a more rapid instability (e.g. Youdin & Shu 2002). Another mechanism that may result in an inner hole and planetesimals at a particular location is the direct or rapid formation of planetesimals in the spiral arms of a self-gravitating disk (Rice et al. 2006; Clarke & Lodato 2009). This process necessarily occurs beyond tens of AU where the disk is marginally stable and dust may be concentrated in spiral arms on a timescale shorter than the orbital period. This process may result in narrow belts, because at $\gtrsim 100$ AU distances the disk is unstable to fragmentation and may form companions that truncate the disk. However, given that only $\sim 10\%$ of the Su et al. (2006) sample have known companions, binary truncation seems an unlikely process for setting disk outer radii.

The alternative is that the belts are locations where systems are able to retain planetesimals. For example, one possibility is truncation by exterior stellar compan-

ions, or within a cluster environment. However, stellar flybys are unlikely to be what sets disk outer radii because the cross section for a close encounter suggests that this mechanism should more often result in large disks, rather than small ones.

Planet formation provides a possible explanation of debris disk radii, and is naturally consistent with both self-stirring and planet-stirring models. It is reasonable to think that planetesimals form out to radii some fraction farther than where planets can form. Dynamical clearing by planets can then set disk inner radii, analogous to how Solar System planets dictate the Asteroid and Kuiper belt locations. In this picture debris disk systems therefore consist of an inner planetary system with some radial extent and a narrow planetesimal belt that extends somewhat further. This picture is essentially that of the planet-stirred example that reproduces the A-star statistics above in §5.1.

The range and distribution of disk radii may be linked to the initial protoplanetary disk mass. Higher surface density disks are expected to form more giant planets over a wider range of radii (e.g. Kennedy & Kenyon 2008) and these systems are likely more susceptible to scattering, resulting in more extended dynamical clearing and debris disks with larger inner radii (and provides a simplistic explanation for why the BPMG and TW Hydrae A-star disks with the largest excesses have the largest radii as discussed below). If most protoplanetary disks are relatively low mass (e.g. Andrews & Williams 2005), this scenario would also typically result in debris disks at relatively small radii in agreement with the r_{24-70} from our A-star sample.

The degree to which planets influence debris disk structure probably varies. In some cases planets may simply dynamically clear inner regions while the rest of the disk is self-stirred, whereas in other cases the disk structure may be entirely set by migration and shepherding, scattering, and secular stirring. We now turn to a small sample of resolved A-stars that allow us to study these possibilities for individual systems.

5.3 Comparison with resolved imaging

Resolved debris disks that show structures such as warps and offsets reveal planets that may remain otherwise invisible. In these cases, planet-stirring is probably more important than self-stirring. Therefore, resolved imaging allows estimation of the stirring mechanism in individual cases.

Resolved imaging also allows other comparisons between observations and models to be made, such as with the surface density profiles shown in Figure 2. Though the distribution of radii in our model is set by comparing model and observed r_{24-70} , this measure tends to underestimate disk radii and cannot account for disks with several dust components, providing further motivation for imaging.

As a sample of resolved debris disks, we use stars in the ~ 12 Myr old β Pic Moving Group (BPMG, Zuckerman & Song 2004) and the similarly aged ~ 8 Myr old TW Hydrae Association. This sample is therefore

Table 1. BPMG and TW Hydrae A-stars with disks. Inferred disk radii r_{24-70} and $f = L_{\text{disk}}/L_{\star}$ from Wyatt et al. (2007b). Real disk radii r_{real} are derived from imaging and modelling (β Pic and HR 4796A, Augereau et al. 2001; Telesco et al. 2005; Schneider et al. 1999, 2009) or detailed SED modelling (Chen et al. 2006; Smith et al. 2009). The fractional luminosities $R_{24} = F_{24,\text{tot}}/F_{24,\star}$ are from Rebull et al. (2008) and Rieke et al. (2005).

Name	r_{24-70} (AU)	r_{real} (AU)	$L_{\text{disk}}/L_{\star}$	R_{24}
HR 4796A	27	70	330e-5	97
β Pic	24	70	140e-5	26
HR 7012	4	0.9, 6	50e-5	5.9
η Tel	25	3.9, 24	20e-5	5.5

roughly coeval and about the age of the $24\ \mu\text{m}$ excess peak.

The A-stars in this sample are HR 4796A (HD 109573), β Pic (HD 39060), η Tel (HD 181296), HR 7012 (HD 172555), HR 6070 (HD 146624), and HR 6749/HR 6750 (HD 165189/HD 165190). Of these, HR 6070 and HR 6749/6750 have no excesses at 24 or $70\ \mu\text{m}$ (Rebull et al. 2008). Characteristics of the remaining four are shown in Table 1. The actual radii (r_{real}) of HR 4796A and β Pic are several times larger than r_{24-70} , and in reasonable agreement for HR 7012 and the outer dust component of η Tel. The difference in the case of β Pic and HR 4796A is explained by the presence of small grains, which emit inefficiently at long wavelengths, and are thus hotter than a blackbody grain at the same stellocentric distance.

Compared to the entire A-star sample, the $24\ \mu\text{m}$ excesses in this 10 Myr sample are among the largest (see Fig. 4). Comparing the fraction of stars with disks with $R_{24} \geq 5.5$ (i.e. the same or brighter than η Tel), the ~ 10 Myr sample has $67 \pm 33\%$ (4/6) while the fraction for the remaining stars in the 6–20 Myr age bin in the overall A-star sample is $8 \pm 5\%$ (3/38). Whether this relatively high excess fraction is the result of evolution within a low density association or simply due to a small sample size is unclear.

Starting with β Pic, this star harbours the second brightest known debris disk, which appears extended in both scattered light and at IR and longer wavelengths (e.g. Smith & Terrile 1984; Chini et al. 1991; Holland et al. 1998; Telesco et al. 2005). The disk appears over a wide range of radii, at least partly due to blowout of small grains created in collisions (Augereau et al. 2001). Modelling of the scattered light and mid-IR emission suggests that the parent disk where these grains originate is centred at around 70–80 AU (Augereau et al. 2001; Telesco et al. 2005). In addition, a $\sim 10 M_{\text{Jup}}$ planet at ~ 10 AU has been inferred as the cause of a warp in the disk (Mouillet et al. 1997) that reaches a peak near the same location as the parent belt (Heap et al. 2000). This proposed companion has recently been imaged (Lagrange et al. 2009a), though confirmation with second epoch observations is needed (Lecavelier Des Etangs & Vidal-Madjar 2009;

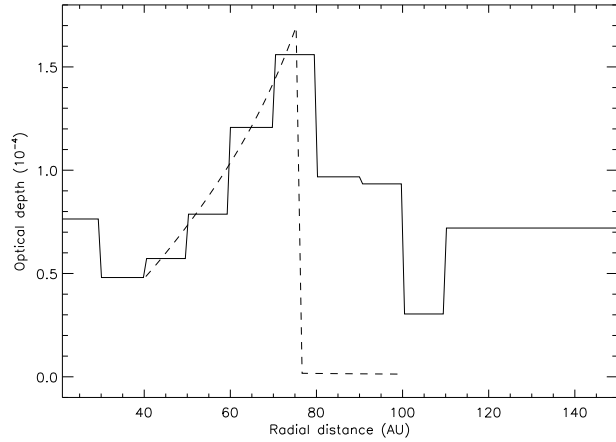


Figure 9. Optical depth in the β Pictoris debris disk derived from Mid-IR imaging (Telesco et al. 2005). Overplotted is the τ_{eff} profile for a secular-stirred planetesimal belt (dashed line) between 40–100 AU (see text for details).

Lagrange et al. 2009b). Finally, Telesco et al. (2005) find an apparent clump of small grains in the South-West wing of the disk at ~ 50 AU.

The solid line in Figure 9 shows the optical depth profile of β Pic derived from mid-IR imaging of β Pic (North-East wing, Telesco et al. 2005). The optical depth peaks at around 75 AU, with a decrease to larger and smaller radii. This profile suggests that the disk has been stirred to 75 AU. Comparison with Figure 2 suggests that the profile is more akin to a fast self-stirred disk because the profile drops immediately interior to 75 AU. That is, the collisional time is shorter than the stirring time at r_{stir} so Condition (10) is not satisfied. As discussed in §3.2 this profile is unlikely to be the result of self-stirring (though can be fit with a self-stirred model).

There are, of course, other possible explanations for the origin of the β Pic optical depth profile. The surface density of small grains interior to 75 AU may drop more rapidly due to continued accretion and stirring by Pluto-size objects for example. Alternatively, if we still assume that the profile is due to collisional evolution, planet-stirring is a possible scenario. As noted in §5.1, this evolution can produce disks that stir in the fast mode. Indeed, a planet has already been proposed as the cause for a warp in the β Pic disk, and the maximum extent of the warp suggests that stirring due to the planet has reached ~ 75 AU, the location of the peak optical depth.

The dashed line in Figure 9 shows the optical depth profile of a planet-stirred model with good agreement between 40–80 AU. The model has a planet with mass $M_{\text{pl}}/M_{\odot} = 16 \times 10^{-3}$ at $a_{\text{pl}} = 10$ AU with $e_{\text{pl}} = 0.1$, and the disk is therefore stirred to ~ 75 AU in 12 Myr (though Eq. 12 shows that M_{pl} , a_{pl} , & e_{pl} are degenerate in setting t_{stir}). The value $e = 0.025$ is roughly the forced eccentricity set by the planet which in turn sets the collision velocities as $\sim 150\ \text{m s}^{-1}$. For the disk to be depleted interior to 75 AU we need fairly small planetesimals, with $D_c = 0.1\ \text{km}$, $Q_D^* = 40\ \text{J kg}^{-1}$, and $\eta = 0.01$. To match the overall level of optical depth requires decreasing q to 1.8 (from 1.83). The collision velocities may

be higher due to increased planetesimal inclinations, expected if the planet is inclined relative to the disk, which is the interpretation of the observed warp (Mouillet et al. 1997; Augereau et al. 2001). In this case, a model with larger planetesimals can reproduce the observed optical depth profile.

To match the optical depth exterior to 80 AU requires very large $x_{\text{delay}} \sim 0.5$. It is more likely that the emission outside 80 AU is due to small grains created in collisions at <80 AU being blown out of the system, thus making the disk appear more extended than it really is (Augereau et al. 2001). Because we infer small D_c , an alternative explanation for the clump of small grains in the South-West wing at about 50 AU is needed, because the clump has about as much mass as a 100 km planetesimal (Telesco et al. 2005). Collective phenomena such as resonance trapping (Wyatt 2003) or dust avalanches (Grigorieva et al. 2007) would be required to explain the clump.

The disk around HR 4796A has a similar radius to β Pic. Detailed modelling suggests a ~ 15 AU wide parent belt at 70 AU with a wider distribution of smaller blowout grains (Wahhaj et al. 2005). As with β Pic, this disk is unlikely to be self-stirred. The relatively sharp inner disk edge and a brightness asymmetry and possible offset (e.g. Telesco et al. 2000; Wahhaj et al. 2005; Schneider et al. 2009), make HR 4796A reminiscent of the Fomalhaut disk, which is known to harbour an interior planet that may affect the disk (Chiang et al. 2009). If the inner edge of the HR 4796A disk is truncated by a planet then it is probably stirred by that planet.

The two remaining disks, those around HR 7012 and η Tel are fainter than the previous two, but still have large excesses relative to the overall A-star sample. HR 7012 has a very small disk, with detailed models of IRS spectra suggesting grain temperatures corresponding to 0.9–6 AU (Chen et al. 2006). These models require sub- μm -sized grains, with a composition indicative of dust produced in a recent collision (Chen et al. 2006; Lisse et al. 2009). The mass of grains inferred is of order 10^{21} g, the mass contained in a planetesimal a few tens of km in diameter. This disk has an unusually small radius for its age (Wyatt et al. 2007b) and a reasonably high $f/f_{\text{max}} \sim 100$, also suggesting that the dust is likely transient and not due to self-stirring. However, this conclusion does not mean that the disk was never self-stirred. To have reached what may be an analogous stage to the giant-impact period that formed the Solar-System’s terrestrial planets, objects orbiting HR 7012 almost certainly went through the stages of growth where self-stirring is expected. This late stage of chaotic growth could be considered a second phase of self-stirring, where the stirring this time arises because the surface density of smaller objects is insufficient to damp the largest objects and big objects stir each other.

Finally, η Tel has distinct planetesimal belts at ~ 4 and 24 AU, each contributing about equally to the excess at $24 \mu\text{m}$. (Chen et al. 2006; Smith et al. 2009). Smith et al. (2009) find that the outer disk can be explained by a self-stirred model. If stirring has reached 24 AU, the hotter dust may be the result of a collision as planets continue to grow in inner regions. In contrast to

HR 7012 however, there is no evidence for sub- μm grains in the η Tel disk from which it might be inferred that a recent collision is required to explain short lived dust (Chen et al. 2006).

In summary, when confronted with detailed observations, the self-stirring model appears to face competition from the continued growth of planets through stochastic collisions and their dynamical effects in trying to provide explanations of disk structure. The β Pic disk is likely stirred by the proposed planet at ~ 10 AU. The non-azimuthal symmetry of the HR 4796A disk also suggests a planetary influence. The η Tel disk is consistent with a self-stirring model and HR 7012 is probably a transient disk resulting from a recent collision.

6 CONCLUSIONS

Recent observations of young A-stars show evidence for an increase in the level and frequency of $24 \mu\text{m}$ excesses from ~ 3 to 10–30 Myr (Hernández et al. 2006; Currie et al. 2008a,b). Excesses then decline on a timescale of ~ 150 yr (Rieke et al. 2005). The rise in debris disk emission at early times has been interpreted as evidence for self-stirring, where a collisional cascade begins when Pluto-size objects form and stir planetesimals. Because the time taken to form Plutos increases with radial distance from the central star, Wyatt (2008) noted that the 10–30 Myr delay also implied that A-star disks must have inner holes of order 10 AU if they are self-stirred. Though there is in fact little evidence that the fraction of stars with $24 \mu\text{m}$ excesses changes in the first 50 Myr or so (Fig. 4), the overall trend shown by the A-star statistics provides tentative observational evidence of self-stirring. However, a promising alternative to self-stirring should also be considered, that debris disks are instead stirred by secular perturbations from an eccentric planet (Mustill & Wyatt 2009).

In this paper, we use the analytic model described in §2 to study the evolution of self-stirred disks. Our model is essentially the steady-state evolution model of Wyatt et al. (2007b), modified to include self-stirring. We first compare our model to the detailed Kenyon & Bromley (2008) results, using an empirical delay for self-stirring to ensure we reproduce their excess trends over a range of disk surface densities and stellar masses (§3). The only difference in evolution is after the peak excess, with the Kenyon & Bromley models decaying more rapidly at $70 \mu\text{m}$, probably due to continued accretion.

We illustrate the implications of collisional evolution for resolved disks (§3.2). Because disks process their mass from the inside out, the surface density profile of any collisionally evolved disk region increases as $r^{7/3}$ and disks appear to increase in radius over time (pre- and planet-stirred disks show the same behaviour). The primordial surface density profile remains where the disk has not been stirred (and protoplanetary growth is ongoing).

Disks with delayed stirring can evolve in two different ways. If the collisional time is short compared to the stirring time (i.e. has more mass than it would if it were pre-stirred) then the disk rapidly loses mass as it

reverts to its equilibrium state. This evolution results in a bright narrow ring of emission where stirring is occurring (Fig. 2). While we suggest that this evolution is unlikely for self-stirred disks, it can occur for planet-stirred disks. Disks that stir before the collisional time evolve in the same way as pre-stirred disks, with the difference that there is less emission in exterior regions where the collisional cascade has not started. This is the typical evolution we expect for self-stirred disks.

In §4, we turn to the observations and show why the pre-stirred debris disk model fails to produce the trends in the A-star statistics; with no mechanism to delay the onset of stirring, $24\ \mu\text{m}$ excesses in the model are highest at the earliest times. The overall fraction of stars with disks declines monotonically with time in contrast with the observations, which peak around 30 Myr. Using the same power-law planetesimal belt radius distribution as Wyatt et al. (2007b), and planetesimal sizes and eccentricities consistent with the Kenyon & Bromley (2008) models, we show that the A-star trends and statistics can be reasonably reproduced by a self-stirring model with $Q_{\text{D}}^* = 45\ \text{J kg}^{-1}$ and the average disk mass 0.15 times an MMSN disk. Disks are “narrow belts” with width $dr = r_{\text{mid}}/2$. The smallest planetesimal belt has $r_{\text{mid}} = 15\ \text{AU}$, and the largest 120 AU.

We have less success fitting the A-star observations with extended disks—disks with fixed inner and/or outer radii. Although the $24\ \mu\text{m}$ emission can be reasonably reproduced with disks with fixed $\sim 150\ \text{AU}$ outer radii and fixed or variable inner radii, these models result in too many $70\ \mu\text{m}$ excess disks at late times. This problem arises because extended disks evolve at near constant $70\ \mu\text{m}$ fractional luminosity until their outer edges are stirred (Figs. 1 & 3). Disks with fixed inner radii of $\sim 15\ \text{AU}$ and variable outer radii also fail to fit the observed statistics, because the models over-predict the number of disks with small radii. Thus, our conclusion that debris disks are narrow belts and not extended is independent of the A-star trends for ages $\lesssim 50\ \text{Myr}$.

Progress can be made in several directions to further understand the effects of self-stirring on model populations. Our model only removes dust from the small end of the size distribution, whereas the Kenyon & Bromley (2008) models show that mass is also lost as Pluto-size objects continue to accrete fragments, and that mass loss is accelerated as the largest objects continue to grow. A model including continued accretion and stirring will lower $70\ \mu\text{m}$ excesses for the oldest disks, perhaps allowing extended disks to reproduce the A-star statistics. However, the Kenyon & Bromley (2009) model comparison with A-star data suggests there will still be difficulties, with extended disk models that include continued accretion and stirring also evolving too slowly at $70\ \mu\text{m}$.

Planets probably stir and set the structure of some disks. In §5.1 we show the A-star statistics can be fit with a population of narrow belts stirred by secular perturbations from an eccentric planet. The planet-stirred model produces essentially the same results as the self-stirred one, with the key to reproducing the A-star observations apparently being the planet location. If planets are located too far from the disk then stirring occurs too late and the characteristic $\sim 150\ \text{Myr}$ timescale decay of $24\ \mu\text{m}$

excesses does not occur. Thus, the successful model has $0.5 M_{\text{Jup}}$ planets with $e = 0.1$ that are located at one third the disk radius.

Therefore, population models cannot yet distinguish whether self-stirring or planet-stirring is more important. Population models are also unlikely to rule out one stirring mechanism due to the many model parameters. The poor statistics for A-stars younger than $\sim 50\ \text{Myr}$ also hinder progress. The fact that the rise in $24\ \mu\text{m}$ excesses for young A-stars has marginal statistical significance is unlikely to change in the near future, as most nearby regions have been studied with *Spitzer* and a significant increase in numbers awaits the launch of JWST.

In §5.2 we consider the origin of narrow planetesimal belts, and suggest that planet formation provides a natural explanation, if planetesimals form to radii somewhat larger than planets. The debris disk inner holes are then regions cleared by planets, and the outer extent set by where planetesimals can form. Depending on planetary system architecture, these planets may also stir the disk as suggested by our planet-stirred example in §5.1.

In §5.3, we look more closely at the sample of $\sim 10\ \text{Myr}$ old resolved disks around A-stars from the BPMG and the TW Hydrae Association, and find that only $\eta\ \text{Tel}$ allows a reasonable explanation with a self-stirring model. The disks around $\beta\ \text{Pic}$ and HR 4796A seem more likely to be affected by planets. It is possible that the $\beta\ \text{Pic}$ debris disk is stirred through secular perturbations from the planet proposed to orbit at $\sim 10\ \text{AU}$. The disk around HR 7012 appears transient, though probably went through a phase of self-stirring when it was younger. These observations suggest that the degree to which debris disks are influenced by planets varies, and that the answer to the question of debris disk stirring lies with high resolution imaging.

ACKNOWLEDGEMENTS

It is a pleasure to thank Ken Rice for helpful discussions, Scott Kenyon for discussions and kindly sharing output from his self-stirring models, and Alexander Krivov for a thorough review that improved the content and presentation of this contribution. This study was completed during the Isaac Newton Institute’s Dynamics of Disks and Planets programme in Cambridge, UK.

REFERENCES

- Alexander, R. D. & Armitage, P. J. 2007, MNRAS, 375, 500 [ADS]
- Andrews, S. M. & Williams, J. P. 2005, ApJ, 631, 1134 [ADS]
- . 2007, ApJ, 671, 1800 [ADS]
- Augereau, J. C., Nelson, R. P., Lagrange, A. M., Papaloizou, J. C. B., & Mouillet, D. 2001, A&A, 370, 447 [ADS]
- Blum, J. & Wurm, G. 2008, ARA&A, 46, 21 [ADS]
- Booth, M., Wyatt, M. C., Morbidelli, A., Moro-Martín, A., & Levison, H. F. 2009, MNRAS, 399, 385 [ADS]

- Burns, J. A., Lamy, P. L., & Soter, S. 1979, *Icarus*, 40, 1 [ADS]
- Carpenter, J. M., Mamajek, E. E., Hillenbrand, L. A., & Meyer, M. R. 2009, *ApJ*, 705, 1646 [ADS]
- Chen, C. H., Sargent, B. A., Bohac, C., Kim, K. H., Leibensperger, E., Jura, M., Najita, J., Forrest, W. J., Watson, D. M., Sloan, G. C., & Keller, L. D. 2006, *ApJS*, 166, 351 [ADS]
- Chiang, E., Kite, E., Kalas, P., Graham, J. R., & Clampin, M. 2009, *ApJ*, 693, 734 [ADS]
- Chini, R., Kruegel, E., Kreysa, E., Shustov, B., & Tutukov, A. 1991, *A&A*, 252, 220 [ADS]
- Clarke, C. J. & Lodato, G. 2009, *MNRAS*, 398, L6 [ADS]
- Currie, T., Kenyon, S. J., Balog, Z., Rieke, G., Bragg, A., & Bromley, B. 2008a, *ApJ*, 672, 558 [ADS]
- Currie, T., Plavchan, P., & Kenyon, S. J. 2008b, *ApJ*, 688, 597 [ADS]
- Dermott, S. F., Grogan, K., Durda, D. D., Jayaraman, S., Kehoe, T. J. J., Kortenkamp, S. J., & Wyatt, M. C. E. Grun, B. A. S. Gustafson S. F. Dermott & H. Fechtig (Berlin:Springer-Verlag), 569–639
- Dohnanyi, J. S. 1969, *J. Geophys. Res.*, 74, 2531 [ADS]
- Dominik, C. & Decin, G. 2003, *ApJ*, 598, 626 [ADS]
- Gomes, R., Levison, H. F., Tsiganis, K., & Morbidelli, A. 2005, *Nature*, 435, 466 [ADS]
- Grigorieva, A., Artymowicz, P., & Thébault, P. 2007, *A&A*, 461, 537 [ADS]
- Haisch, Jr., K. E., Lada, E. A., & Lada, C. J. 2001, *ApJ*, 553, L153 [ADS]
- Heap, S. R., Lindler, D. J., Lanz, T. M., Cornett, R. H., Hubeny, I., Maran, S. P., & Woodgate, B. 2000, *ApJ*, 539, 435 [ADS]
- Hernández, J., Briceño, C., Calvet, N., Hartmann, L., Muzerolle, J., & Quintero, A. 2006, *ApJ*, 652, 472 [ADS]
- Hernández, J., Calvet, N., Hartmann, L., Muzerolle, J., Gutermuth, R., & Stauffer, J. 2009, *ApJ*, 707, 705 [ADS]
- Hernández, J., Hartmann, L., Calvet, N., Jeffries, R. D., Gutermuth, R., Muzerolle, J., & Stauffer, J. 2008, *ApJ*, 686, 1195 [ADS]
- Hernández, J., Hartmann, L., Megeath, T., Gutermuth, R., Muzerolle, J., Calvet, N., Vivas, A. K., Briceño, C., Allen, L., Stauffer, J., Young, E., & Fazio, G. 2007, *ApJ*, 662, 1067 [ADS]
- Holland, W. S., Greaves, J. S., Zuckerman, B., Webb, R. A., McCarthy, C., Coulson, I. M., Walther, D. M., Dent, W. R. F., Gear, W. K., & Robson, I. 1998, *Nature*, 392, 788 [ADS]
- Johnson, J. A., Butler, R. P., Marcy, G. W., Fischer, D. A., Vogt, S. S., Wright, J. T., & Peek, K. M. G. 2007, *ApJ*, 670, 833 [ADS]
- Kalas, P., Graham, J. R., Chiang, E., Fitzgerald, M. P., Clampin, M., Kite, E. S., Stapelfeldt, K., Marois, C., & Krist, J. 2008, *Science*, 322, 1345 [ADS]
- Kalas, P., Graham, J. R., Clampin, M. C., & Fitzgerald, M. P. 2006, *ApJ*, 637, L57 [ADS]
- Kennedy, G. M. & Kenyon, S. J. 2008, *ApJ*, 673, 502 [ADS]
- 2009, *ApJ*, 695, 1210 [ADS]
- Kenyon, S. J. & Bromley, B. C. 2004, *AJ*, 127, 513 [ADS]
- 2008, *ApJS*, 179, 451 [ADS]
- 2009, ArXiv e-prints, (0911.4129) [ADS]
- Kharchenko, N. V. 2001, *Kinematika i Fizika Nebesnykh Tel*, 17, 409 [ADS]
- Lagrange, A., Gratadour, D., Chauvin, G., Fusco, T., Ehrenreich, D., Mouillet, D., Rousset, G., Rouan, D., Allard, F., Mendron, É., Charton, J., Mugnier, L., Rabou, P., Montri, J., & Lacombe, F. 2009a, *A&A*, 493, L21 [ADS]
- Lagrange, A., Kasper, M., Boccaletti, A., Chauvin, G., Gratadour, D., Fusco, T., Ehrenreich, D., Apai, D., Mouillet, D., & Rouan, D. 2009b, *A&A*, 506, 927 [ADS]
- Lecavelier Des Etangs, A. & Vidal-Madjar, A. 2009, *A&A*, 497, 557 [ADS]
- Leinhardt, Z. M. & Stewart, S. T. 2009, *Icarus*, 199, 542 [ADS]
- Lissauer, J. J. 1987, *Icarus*, 69, 249 [ADS]
- Lisse, C. M., Chen, C. H., Wyatt, M. C., Morlok, A., Song, I., Bryden, G., & Sheehan, P. 2009, *ApJ*, 701, 2019 [ADS]
- Löhne, T., Krivov, A. V., & Rodmann, J. 2008, *ApJ*, 673, 1123 [ADS]
- McCaughrean, M. J. & O’dell, C. R. 1996, *AJ*, 111, 1977 [ADS]
- Morbidelli, A., Bottke, W. F., Nesvorný, D., & Levison, H. F. 2009, *Icarus*, 204, 558 [ADS]
- Moro-Martín, A. & Malhotra, R. 2003, *AJ*, 125, 2255 [ADS]
- Mouillet, D., Larwood, J. D., Papaloizou, J. C. B., & Lagrange, A. M. 1997, *MNRAS*, 292, 896 [ADS]
- Mustill, A. J. & Wyatt, M. C. 2009, *MNRAS*, 399, 1403 [ADS]
- Najita, J. & Williams, J. P. 2005, *ApJ*, 635, 625 [ADS]
- Natta, A., Grinin, V., & Mannings, V. 2000, *Protostars and Planets IV*, 559 [ADS]
- Quillen, A. C. 2006, *MNRAS*, 372, L14 [ADS]
- Quillen, A. C., Morbidelli, A., & Moore, A. 2007, *MNRAS*, 380, 1642 [ADS]
- Rebull, L. M., Stapelfeldt, K. R., Werner, M. W., Mannings, V. G., Chen, C., Stauffer, J. R., Smith, P. S., Song, I., Hines, D., & Low, F. J. 2008, *ApJ*, 681, 1484 [ADS]
- Rhee, J. H., Song, I., Zuckerman, B., & McElwain, M. 2007, *ApJ*, 660, 1556 [ADS]
- Rice, W. K. M., Lodato, G., Pringle, J. E., Armitage, P. J., & Bonnell, I. A. 2006, *MNRAS*, 372, L9 [ADS]
- Rieke, G. H., Su, K. Y. L., Stansberry, J. A., Trilling, D., Bryden, G., Muzerolle, J., White, B., Gorlova, N., Young, E. T., Beichman, C. A., Stapelfeldt, K. R., & Hines, D. C. 2005, *ApJ*, 620, 1010 [ADS]
- Schmidt-Kaler, T. in , *Landolt-Bornstein: Numerical Data and Functional Relationships in Science and Technology, Group VI*, ed. K. Schaifers H. H. Voigt, Vol. 2 (Berlin:Springer-Verlag) [LINK]
- Schneider, G., Smith, B. A., Becklin, E. E., Koerner, D. W., Meier, R., Hines, D. C., Lowrance, P. J., Terrile, R. J., Thompson, R. I., & Rieke, M. 1999, *ApJ*, 513, L127 [ADS]
- Schneider, G., Weinberger, A. J., Becklin, E. E., Debes, J. H., & Smith, B. A. 2009, *AJ*, 137, 53 [ADS]
- Siegler, N., Muzerolle, J., Young, E. T., Rieke, G. H., Mamajek, E. E., Trilling, D. E., Gorlova, N., & Su, K. Y. L. 2007, *ApJ*, 654, 580 [ADS]

- Smith, B. A. & Terrile, R. J. 1984, *Science*, 226, 1421 [\[ADS\]](#)
- Smith, R., Churcher, L. J., Wyatt, M. C., Moerchen, M. M., & Telesco, C. M. 2009, *A&A*, 493, 299 [\[ADS\]](#)
- Su, K. Y. L., Rieke, G. H., Stansberry, J. A., Bryden, G., Stapelfeldt, K. R., Trilling, D. E., Muzerolle, J., Beichman, C. A., Moro-Martin, A., Hines, D. C., & Werner, M. W. 2006, *ApJ*, 653, 675 [\[ADS\]](#)
- Telesco, C. M., Fisher, R. S., Piña, R. K., Knacke, R. F., Dermott, S. F., Wyatt, M. C., Grogan, K., Holmes, E. K., Ghez, A. M., Prato, L., Hartmann, L. W., & Jayawardhana, R. 2000, *ApJ*, 530, 329 [\[ADS\]](#)
- Telesco, C. M., Fisher, R. S., Wyatt, M. C., Dermott, S. F., Kehoe, T. J. J., Novotny, S., Mariñas, N., Radomski, J. T., Packham, C., De Buizer, J., & Hayward, T. L. 2005, *Nature*, 433, 133 [\[ADS\]](#)
- Wahhaj, Z., Koerner, D. W., Backman, D. E., Werner, M. W., Serabyn, E., Ressler, M. E., & Lis, D. C. 2005, *ApJ*, 618, 385 [\[ADS\]](#)
- Watson, A. M., Stapelfeldt, K. R., Wood, K., & Ménard, F. 2007, *Protostars and Planets V*, 523 [\[ADS\]](#)
- Weidenschilling, S. J. 1977, *Ap&SS*, 51, 153 [\[ADS\]](#)
- Wyatt, M. C. 2003, *ApJ*, 598, 1321 [\[ADS\]](#)
- . 2005, *A&A*, 433, 1007 [\[ADS\]](#)
- . 2008, *ARA&A*, 46, 339 [\[ADS\]](#)
- Wyatt, M. C. & Dent, W. R. F. 2002, *MNRAS*, 334, 589 [\[ADS\]](#)
- Wyatt, M. C., Dermott, S. F., Telesco, C. M., Fisher, R. S., Grogan, K., Holmes, E. K., & Piña, R. K. 1999, *ApJ*, 527, 918 [\[ADS\]](#)
- Wyatt, M. C., Smith, R., Greaves, J. S., Beichman, C. A., Bryden, G., & Lisse, C. M. 2007a, *ApJ*, 658, 569 [\[ADS\]](#)
- Wyatt, M. C., Smith, R., Su, K. Y. L., Rieke, G. H., Greaves, J. S., Beichman, C. A., & Bryden, G. 2007b, *ApJ*, 663, 365 [\[ADS\]](#)
- Yi, S., Demarque, P., Kim, Y., Lee, Y., Ree, C. H., Lejeune, T., & Barnes, S. 2001, *ApJS*, 136, 417 [\[ADS\]](#)
- Youdin, A. N. & Shu, F. H. 2002, *ApJ*, 580, 494 [\[ADS\]](#)
- Zuckerman, B. & Song, I. 2004, *ARA&A*, 42, 685 [\[ADS\]](#)